Dynamic metabolic rewiring enables efficient acetyl-CoA assimilation in *Paracoccus denitrificans*

Katharina Kremer[a], Muriel C.F. van Teeseling[b], Lennart Schada von Borzyskowski[a], Iria Bernhardsgrütter[a], Rob J. M. van Spanning[c], Andrew J. Gates[d], Mitja N.P. Remus-Emsermann[e,f], Martin Thanbichler[a,b,g], and Tobias J. Erb[a,b,g] (*)

[a] Max Planck Institute for Terrestrial Microbiology, Marburg, 35043, Germany
[b] Faculty of Biology, Philipps-Universität, Marburg, 35043, Germany
[c] Department of Molecular Cell Biology, Vrije Universiteit, HV Amsterdam, 1081, The Netherlands
[d] School of Biological Sciences, University of East Anglia, Norwich Research Park, Norwich, NR4 7TJ, U.K.
[e] School of Biological Sciences, University of Canterbury, Christchurch, 8140, New Zealand
[f] Biomolecular Interaction Centre, University of Canterbury, Christchurch, 8140, New Zealand
[g] LOEWE Center for Synthetic Microbiology, Marburg, 35043, Germany

Running Head: Metabolic rewiring in *P. denitrificans*

*Address correspondence to Tobias J. Erb: toerb@mpi-marburg.mpg.de.

Word counts:

Abstract: 225
Importance: 116

Text (excluding references, table footnotes, figure legends): 4370

ABSTRACT

During growth, microorganisms have to balance metabolic flux between energy and biosynthesis. One of the key intermediates in central carbon metabolism is acetyl-CoA, which can be either oxidized in the citric acid cycle or assimilated into biomass through dedicated pathways. Two acetyl-CoA assimilation strategies have been described in bacteria so far, the ethylmalonyl-CoA pathway (EMCP) and the glyoxylate cycle (GC). Here, we show that *Paracoccus denitrificans* uses both strategies for acetyl-CoA assimilation during different growth stages, revealing an unexpected metabolic complexity in the organism's central carbon metabolism. The EMCP is constitutively expressed on various substrates and leads to high biomass yields on substrates requiring acetyl-CoA assimilation, such as acetate, while the GC is specifically induced on these substrates, enabling fast growth rates. Even though each acetyl-CoA assimilation strategy alone confers a distinct growth advantage, *P. denitrificans* recruits both to adapt to changing environmental conditions, such as a switch from succinate to acetate. Time-resolved single-cell experiments show that during this switch, expression of the EMCP and GC is highly coordinated, indicating fine-tuned genetic programming. The dynamic metabolic rewiring of acetyl-CoA assimilation is an evolutionary innovation by *P. denitrificans* that allows this organism to respond in a highly flexible manner to changes in the nature and availability of the carbon source to meet the physiological needs of the cell, representing a new phenomenon in central carbon metabolism.

IMPORTANCE

Central carbon metabolism provides organisms with energy and cellular building blocks during growth and is considered as the invariable 'operating system' of the cell. Here we describe a new phenomenon in bacterial central carbon metabolism. In contrast to many other bacteria, that employ only one pathway for the conversion of the central metabolite acetyl-CoA, *Paracoccus denitrificans* possesses two different acetyl-CoA assimilation pathways. These two pathways are dynamically recruited during different stages of growth, which allows *P. denitrificans* to achieve both high biomass yield and fast growth rates under changing environmental conditions. Overall this dynamic rewiring of central carbon metabolism in *P. denitrificans* represents a new strategy compared to other organisms employing only one acetyl-CoA assimilation pathway.

Introduction

During growth, bacteria have to distribute metabolic flux between catabolism and anabolism. An important central metabolic pathway is the tricarboxylic acid (TCA) cycle, which interfaces anabolism and catabolism. In the TCA cycle, the C2-unit acetyl-CoA is catabolized into CO_2, generating reducing equivalents and ATP for the cell. At the same time, the TCA cycle produces several intermediates that are committed to biosynthesis.

Note that the TCA cycle poses a special challenge for many compounds that are exclusively metabolized via acetyl-CoA, such as acetate, alcohols, short and long chain-fatty acids, esters and waxes. Because all carbon of acetyl-CoA is lost to CO_2, this allows energy conservation, but not carbon assimilation through the TCA cycle. Consequently, dedicated pathways for the assimilation of acetyl-CoA are required to allow growth on these ubiquitous substrates.

Two different acetyl-CoA assimilation pathways have been described in bacteria: the glyoxylate cycle (GC) (1, 2) and the ethylmalonyl-CoA pathway (EMCP) (3, 4). The GC uses two enzymes in addition to the enzymes of the TCA cycle. The first enzyme of the GC, isocitrate lyase (Icl), cleaves isocitrate into succinate and glyoxylate. This step is followed by the condensation of glyoxylate with a second molecule of acetyl-CoA to form malate and free CoA in a reaction catalyzed by the second enzyme of the GC, malate synthase (1, 2).

The EMCP also forms malate and succinate. However, unlike the GC, the EMCP is a linear pathway that employs 13 different enzymes that collectively convert a total of three acetyl-CoA and two CO_2 molecules into the TCA cycle intermediates malate and succinate. The key enzyme of the EMCP is crotonyl-CoA carboxylase/reductase (Ccr), which catalyzes the reductive carboxylation of crotonyl-CoA to ethylmalonyl-CoA (3-5).

Overall, the GC and the EMCP differ substantially in terms of co-factor and carbon requirements. The GC requires four ATP and generates reducing equivalents on the level of two nicotinamides as well as two quinols per four acetates converted into malate (estimated $\Delta_r G'^0$ = -129 kJ/mol). To generate two malate from acetate in the EMCP, three molecules of acetate and two CO_2 are converted at the expense of three ATP and two reduced nioctinamides, while two quinols are generated

(estimated $\Delta_r G'^0$ = -142 kJ/mol). When acetate is used to generate the CO_2 and fuel the cycle, this changes the stoichiometry to three consumed ATP, and one reduced nicotinamide, as well as three quinols generated (estimated $\Delta_r G'^0$ = -190 kJ/mol). While the EMCP requires more enzymatic steps (and likely more cellular resources), it enables the fixation of inorganic carbon into biomass, as well as the co-assimilation of different C5- and C3-carbonic acids compared to the GC, indicating that the two pathways provide different physiological advantages.In most bacteria, only one of the two acetyl-CoA assimilation pathways is present. Importantly, the alphaproteobacterium *Paracoccus denitrificans* encodes the enzymes for both acetyl-CoA assimilation pathways (Figure 1), raising the question of which role each individual pathway would play in the cell.

In this work, we show that *P. denitrificans* uses both the GC and the EMCP. The EMCP serves as default acetyl-CoA assimilation pathway that is always present with low activity in the cell during growth on various substrates, including carbon sources that do not require acetyl-CoA assimilation. By contrast, the GC is specifically induced after switching to carbon sources that depend on acetyl-CoA assimilation, such as acetate or crotonate. We further demonstrate that the two acetyl-CoA assimilation pathways confer distinct physiological advantages. Growth with the EMCP results in increased biomass yield in *P. denitrificans*, while the GC allows for higher growth rates, suggestive for a rate-yield trade-off between the two pathways. Phylogenetic analysis indicates that *P. denitrificans* and several other alphaproteobacteria acquired the GC through lateral gene transfer, consisting with a specific adaptation of the central carbon metabolism of these organisms during evolution. Collectively, our experiments show a surprising flexibility in central carbon metabolism of alphaproteobacteria that allows the complete rewiring of metabolic flux depending on the type and availability of the carbon and free energy source according to the physiological needs of the cell.

Results

P. denitrificans uses the EMCP and the GC for acetyl-CoA assimilation

Earlier studies suggested that *Paracoccus* might use the EMCP as well as the GC for acetyl-CoA assimilation (4, 6, 7). We therefore searched the genome of the fully sequenced strain *P. denitrificans* Pd1222 for homologs of genes involved in the EMCP and the GC from *Rhodobacter sphaeroides* 2.4.1 and *Escherichia coli* K-12, respectively. Our analysis verified that *P. denitrificans* has the genetic potential for both, the GC as well as the EMCP (Figure 1, Table 1; (4)).

To test whether both the EMCP and the GC are functional and thus operate in *P. denitrificans*, we grew bacterial cells in batch culture on minimal medium supplemented with different carbon sources and quantified the activity of Ccr, the key enzyme of the EMCP, as well as Icl, the key enzyme of the GC, in cell-free extracts obtained from the cultures at mid-log phase (Figure 2).

Activity of Ccr was almost undetectable in cells grown on succinate, and at a very low basal level (<100 mU/mg) in extracts of cells grown on glucose and glycolate. In contrast, the activity of Ccr was significantly higher in extracts of cells grown on crotonate, acetate and ethanol. In these extracts, Icl activity was also present, while no Icl activity was detected in extracts of cells grown on glucose, succinate, and glycolate. Together, our data suggest that both the EMCP and the GC are active in *P. denitrificans*. However, while the EMCP is always active at low levels and upregulated in response to growth on substrates requiring acetyl-CoA assimilation, the GC is specifically activated only during growth of *P. denitrificans* on these substrates.

The EMCP is sufficient to sustain growth of *P. denitrificans* on acetate

Next, we tested whether both pathways are essential for acetyl-CoA assimilation in *P. denitrificans*. To that end we aimed to selectively block the GC or EMCP using external inhibitors. Several inhibitors of Icl are known (8). We screened three of them to identify 3-nitropropionate (3-NPA; (9)) as potential candidate for a selective GC inhibitor of *P. denitrificans in vivo*.

3-NPA inhibited purified *P. denitrificans* Icl *in vitro* with an apparent IC50 of 34 µM at concentrations of 100 µM D,L-isocitrate (Figure 3A). Moreover, 3-NPA did not affect growth of *P. denitrificans* on carbon substrates that do not require Icl activity, such as succinate (Figure 2B; Figure S 1E). Notably, 3-NPA did also not affect growth of *Methylobacterium extorquens* AM1, an EMCP-positive organisms that is closely related to *P. denitrificans*, on acetate (Figure S 1B and E). This suggested to us that 3-NPA acts as GC inhibitor which shows negligible off-target effects in the cell, although additional effects of 3-NPA could not be completely excluded.

When we added increasing concentrations of 3-NPA to *P. denitrificans* growing on acetate, the growth rate was successively decreased from 0.26 ± 0.043 h^{-1} (0 µM 3-NPA) to 0.13 ± 0.005 h^{-1} (600 µM 3-NPA), but not completely abolished (Figure 3B; Figure S 1D. This indicated that the GC is not essential in *P. denitrificans* and that the EMCP is sufficient for acetyl-CoA assimilation.

The use of GC increases the growth rate of *P. denitrificans* on acetate

To estimate the contribution of each pathway to acetyl-CoA assimilation, we individually deleted the genes coding for Ccr and Icl from the genome of *P.*

denitrificans, yielding strains Δ*ccr* and Δ*icl*, respectively (Figure 4, Figure S2). During growth on succinate, both deletion strains grew similar to the wild type. However, a shift from succinate to acetate caused pronounced and different strain-specific growth defects.

Δ*ccr* grew with wild type-like growth rates, but displayed an extended lag phase (Figure 4). Notably, this lag phase ranged from 15 to 50 h between different experiments (Figure S3). However, when the Δ*ccr* strain was sub-cultured on acetate, the variation in the lag phase disappeared (Figure 4B, blue solid line), and the growth rate corresponded to that of the wild type (Figure 4B and C), indicating that the mutant adapted to acetate.

Δ*icl*, in contrast, did not exhibit a prolonged lag phase, but showed a decreased growth rate on acetate, which is consistent with the results of the 3-NPA inhibition experiments. Together, these results suggest that the GC enables fast growth of *P. denitrificans* on acetate, but unlike the EMCP, requires some time to be induced after a switch onto acetate.

EMCP and GC show a complex expression pattern during switches from succinate to acetate

To follow the expression of the EMCP and the GC *in vivo*, the native *ccr* and *icl* genes of *P. denitrificans* were replaced with constructs encoding translational fusions of Ccr to the red fluorescent protein mCherry and Icl to the cyan fluorescent protein Cerulean, respectively. The resulting strain (*P. denitrificans ccr::ccr-mCherry icl::icl-cerulean*) was continuously monitored by following the total fluorescence of the population during cultivation in 96-well plates (Figure 5)

During growth on succinate, cells showed very low levels of mCherry fluorescence and even lower levels of Cerulean fluorescence, which is consistent with our earlier finding that basal Ccr, but no Icl activity could be detected in cell-free extracts of *P. denitrificans* grown on succinate (Figure 2). When shifted from succinate to acetate, the reporter strain showed biphasic *ccr-mCherry* and *icl-cerulean* expression patterns. Ccr-mCherry fluorescence increased within the first 20 h and then decreased gradually at the onset of exponential phase until it again reached a low basal level. By contrast, the production of Icl-Cerulean started only after 20 h, but continued to increase until shortly before the cells entered stationary phase. Subsequently, Icl-Cerulean fluorescence dropped transiently before continuing to rise again in the late stationary phase. Very similar growth-linked expression patterns were observed in reporter strains of *P. denitrificans* carrying only a single Ccr-mCherry or Icl-mCherry fusion (Figure S 5). In summary, our results suggest that acetyl-CoA assimilation in *P. denitrificans* follows a complex regulatory pattern, in which the GC is used for fast and efficient acetyl-CoA assimilation during exponential phase, while the EMCP is used to bypass the time needed for activation of the GC.

Population-wide switch responses monitored by single cell microscopy

To understand whether the transition from EMCP- to GC-driven acetyl-CoA assimilation during the switch to acetate occurred in the whole population or only in a subset of cells, we followed the production of Ccr-mCherry and Icl-Cerulean in *P. denitrificans ccr::ccr-mCherry icl::icl-cerulean* at the single cell level using time-lapse fluorescence microscopy. Here, we imaged cells growing on succinate (Figure 6A and B) and acetate (Figure 6C and D) at two-hour intervals and subjected the images to automated analysis (10) to determine the average fluorescence per cell (Figure 6A and C). While repeated handling of the cultures for sample collection led to slightly decreased growth rates, the overall expression patterns of *ccr-mCherry* and *icl-cerulean* matched those measured during continuous cultivation in the 96-well plates (Figure 5).

While no fluorescence was detected for the wild type (negative control; Figure S 4), the reporter strain showed different production patterns for Ccr-mCherry and Icl-Cerulean. On succinate, Ccr was produced at low levels during exponential phase, with increased expression in the stationary phase. By contrast, Icl was detected only at the end of the exponential phase and only in a small fraction of cells, which appeared strongly fluorescent. This implies Icl expression is heterogeneous in the late exponential phase on succinate, and thus may suggest a bet-hedging-like behavior under these conditions (Figure 6A and B, Figure S 6).

Upon the switch to acetate, Ccr was produced first, whereas Icl was only induced at the onset of the early exponential phase. While some cells switched earlier to Icl production than others, all cells produced Icl in the exponential phase, indicating that the whole population and not only a subset of cells shifted from using the EMCP to the GC (Figure 6C and D, Figure S 6).

To follow the expression dynamics of *ccr* and *icl* continuously in individual cells, we trapped succinate-grown *P. denitrificans ccr::ccr-mCherry icl::icl-cerulean* in a microfluidic device. We then provided acetate as the sole source of carbon and tracked cell growth and division as well as reporter production by microscopy over the course of time (Supplementary Video 1). This analysis confirmed that essentially all cells switched from the EMCP to the GC, demonstrating that faster acetyl-CoA assimilation is switched on in the whole population and not by individual cells that outgrow the population (Figure 7).

Discussion

Here we describe an unprecedented (and unexpected) metabolic redundancy in bacterial central carbon metabolism. The chromosome of *P. denitrificans* carries genes for two fundamentally different acetyl-CoA assimilation pathways, the EMCP and the GC. Both pathways are functional and regulated dynamically depending on the growth stage of the cells. The EMCP serves a default function and is expressed at basal levels at all times and on all carbon and free energy sources tested. Upon a switch to acetate, the EMCP is strongly induced at the early stage of growth but then decreases in activity again. The GC, by contrast, is exclusively induced on acetate and reaches peak activity at the late stage of growth, indicating a surprising rewiring of central carbon metabolism in *P. denitrificans* at the onset of the exponential phase.

What might be the reasons for the rewiring of central carbon metabolism in *P. denitrificans*? Individual knock out strains of the EMCP and GC show that the two pathways confer distinct advantages. The EMCP increases the growth yield, while the GC allows faster growth on acetate. How can these differences be explained and what are their consequences?

Importantly, the EMCP is able to fix inorganic carbon to increase biomass yield according to the following equation: 3 acetate + 2 CO_2 + 2 NADPH + 2 quinones → 2 malate + 2 $NADP^+$ + 2 quinols. This stoichiometry allows organisms using the EMCP to gain extra carbon from the environment if additional reducing equivalents are available to the cell, e.g. through internal storage compounds, such as poly-hydroxybutyrate (PHB), or growth substrates that are comparatively more reduced than average cellular carbon. This is supported by recent calculations that predict an approximately 3% higher yield for *M. extorquens* on methanol when using the EMCP compared to the GC (12). Another important feature of the EMCP is that it does not only enable acetyl-CoA assimilation but is directly linked to PHB metabolism and can also function in the assimilation of propionate, in addition to several dicarboxylic acids. This versatility makes the EMCP an all-purpose pathway that might allow *P. denitrificans* to assimilate several different carbon and free energy sources in parallel, which could explain the constant expression of the EMCP on diverse growth substrates.

The GC on the other hand is a very specialized route that requires only two additional enzymes. The GC requires less protein resources and the thermodynamics of the cycle (i.e., the free energy of the overall process) might become more favorable with the upper limit of free Gibbs energy dissipation rate in *P. denitrificans* (13). Rerouting acetyl-CoA assimilation to the GC thus might allow a higher metabolic flux and consequently faster growth, providing a potential explanation as to why *P. denitrificans* switches to the GC when high concentrations of acetate are available.

Overall, a picture emerges in which metabolic rewiring is a highly coordinated strategy in *P. denitrificans* that allows optimal growth of this species in a changing environment. When the growth substrate changes from succinate to acetate, it is conceivable that the constant expression of the EMCP would facilitate the immediate assimilation of acetate. This could help *P. denitrificans* during the lag phase until the GC is fully induced and thus provide an advantage over other microorganisms that rely on the GC only. Once induced, the GC then could enable increased acetate assimilation rates, which might enable *P. denitrificans* to outcompete microorganisms that solely possess the EMCP.

Out of 48 *Paracoccus* genomes analyzed, 34 possess only a *ccr* homolog, while 9 additionally contain a homolog of *icl* (Figure 8, Figure S 7 and S 8). Only five strains seem to exclusively possess an *icl* homolog. Notably, *ccr* phylogeny largely corresponds to overall strain phylogeny, suggesting that the EMCP is the ancient acetyl-CoA assimilation strategy in the genus *Paracoccus*. This hypothesis is in line with our experimental observation that the EMCP serves a default function in *P. denitrificans* and is further supported by the fact that other, closely related alphaproteobacteria possess only the EMCP (4).

Notably, the phenomenon of metabolic rewiring is presumably not restricted to the *Paracoccus* clade alone. Several alphaproteobacteria show the genetic potential to express multiple acetyl-CoA assimilation pathways (4), suggesting that dynamic rewiring of the central carbon metabolism is a more widespread strategy in nature. This discovery extends recent findings that metabolic degeneracy plays an important role in alphaproteobacterial metabolism (14). Future experiments will focus on understanding the molecular mechanisms that underlie the coordination of the two acetyl-CoA pathways and their regulation through transcriptional, posttranslational or allosteric regulatory mechanisms (15-18), and on clarifying the evolutionary and ecological significance of dynamic metabolic rewiring as new principle in microbial central carbon metabolism.

Acknowledgements

This work was supported by funds from the Germany Research Foundation (Project 192445154 – SFB 987; to T.E. and M.T.). M.C.F.v.T. acknowledges support from the European Molecular Biology Organization (EMBO Long-Term Fellowship ALTF 1396-2015).

Author contributions

K.K., I.B., L.S.v.B., and T.J.E. conceptualized the project. R.v.S. and A.J.G. contributed by giving fundamental advice in molecular biology and training in genetic manipulation of *Paracoccus denitrificans*. K.K and T.J.E. designed the study. K.K. performed all genetic and biochemical experiments and analyses. K.K., M.C.F.v.T. and M.T. planned and performed all microscopic analyses. K.K. and M.N.P.R.E. analysed the microscopic images of the time-lapse experiments. K.K. and L.S.v.B. performed homology and phylogenetic analyses. K.K. and T.J.E. wrote the manuscript.

Declaration of interests

The authors declare no competing interests.

Material and Methods

Strains, media and growth conditions

All experiments were performed with *Paracoccus denitrificans* strains DSM413 or Pd1222. The strain preferentially used for all experiments was DSM413, which is the original wild-type strain isolated by Beijerinck in 1908 (19). In cases where genetic manipulation of this strain was not successful, its genetically more tractable derivative Pd1222 (20), was used alternatively. *P. denitrificans* was grown at 30 °C in mineral salt medium (trace elements: TE3-Zn) (21) supplemented with defined carbon sources and adjusted to a total carbon concentration of 120 mM. The density of cultures was determined photometrically at a wavelength of 600 nm. Bacterial growth

was monitored over time using TECAN Infinite® 200 PRO plate reader systems (Tecan Trading AG, Switzerland) with Nunclon™ Delta Surface 96-well plates (Thermo Scientific, USA). *In silico* analysis of growth data was performed using the software Prism 7 (GraphPad Software, USA). *Escherichia coli* was grown at 37 °C in Luria Bertani Broth or M9 minimal medium (337 mM NaH_2PO_4, 220 mM KH_2PO_4, 85.5 mM NaCl, 18.7 mM NH_4Cl, 1 mM $MgSO_4$, 0.3 mM $CaCl_2$, 0.13 mM Na_2EDTA, 0.03 mM $FeSO_4$, 1 µg/mL biotine, 1 µg/mL thiamine) supplemented with 60 mM acetate. *Methylobacterium extorquens* AM1 was grown at 30 °C in mineral medium as described previously (22) supplemented with 10 mM acetate. Antibiotic concentrations were used as follows: kanamycin at 25 or 50 µg mL^{-1}, spectinomycin at 50 µg mL^{-1}, tetracycline at 10 µg mL^{-1}.

Chemicals

All chemicals were obtained from Sigma-Aldrich (Steinheim, Germany) and Carl Roth (Karlsruhe, Germany), respectively, and were of highest purity available.

Construction of plasmids

Oligonucleotides and synthetic genes were purchased from Eurofins Deutschland (Hamburg, Germany). All standard cloning techniques were carried out according to (25).

Markerless genomic deletions and integrations of reporter genes were generated using the pK18*mobsacB* sucrose suicide plasmid system (26).

For the deletion of *ccr* (*Pden_3873*) and *icl* (*Pden_1363*), respectively, fusions of the respective downstream and upstream flanking regions of the genes, each approximately 700 bp in length, were purchased as synthetic genes cloned into the pEX-K4 backbone (pSYNccrflanks (pTE1602) pSYNiclflanks (pTE1604)). Restriction of the plasmids with PstI and EcoRI, gel-purification of the flanking regions and subsequent ligation into PstI/EcoRI-digested pK18*mobsacB* resulted in plasmids pK18*mobsacB*_ccrflanks (pTE1606) and pK18*mobsacB*_iclflanks (pTE1615).

For the introduction of fluorescent reporter fusions, *ccr* and *icl* were ordered as synthetic genes fused to *evoglowPp1* (27) and *mCherry* (28), respectively, each preceded by a 30-bp linker and followed by the downstream region of the respective genes, yielding plasmids pEX4_ccrevoglowPp1ccrds (pTE1601) and pEX4_iclmCherryicIds (pTE1603).

pTE1603 was digested with SalI and BamHI. Subsequent ligation into SalI/BamHI-cut pK18mobsacB yielded pK18*mobsacB*_iclmCherryicIds (pTE1616).

pTE1601 was amplified with targeted omission of *evoglowPp1* via inverted PCR using primers NdeI_pKK21-f and pKK21-r. *mCherry* was amplified from pTE1603 using primers mCherry-f and NdeI_mCherry-r. Restriction of both fragments with AvrII and NdeI and subsequent ligation of the individual fragments to each other resulted in the plasmid pEX4_ccrmCherryccrds. pEX4-ccrmCherryccrds was digested with SalI and BamHI. Subsequent ligation into SalI/BamHI-cut pK18mobsacB yielded pK18*mobsacB*_ccrmCherryccrds (pTE1624).

pTE1603 was amplified with targeted omission of *mCherry* via inverted PCR using primers NdeI_pSYNiclXicIds-f and HindIII_pSYNccrXccrds-r. *cerulean* (29) was amplified from plasmid pVCERC-6 (30) using primers HindIII_cerulean-f and NdeI_cerulean-r. Restriction of both fragments with HindIII and NdeI and subsequent ligation of the individual fragments to each other resulted in the plasmid

pEX4_iclceruleaniclds. Restriction of pEX4_iclceruleaniclds with SalI and BamHI and ligation into SalI/BamHI-cut pK18*mobsacB* yielded pK18*mobsacB*_iclceruleaniclds (pTE1625).

For the heterologous expression of *icl, icl* was amplified from pTE1603 using primers NdeI_icl-for and HindIII_icl. The resulting product was digested with NdeI and HindIII and ligated into NdeI/HindIII-digested pET16b, yielding pET16b_icl (pTE1614).

Genetic manipulation of *P. denitrificans*

The transfer of plasmids into *P. denitrificans* was achieved by biparental mating with the donor strain *E. coli* ST18 (23). Selection of the first integration was performed on LB or methanol mineral medium plates supplemented with 25 µg/mL kanamycin. Colonies were picked and restreaked on LB with kanamycin and LB with 3% sucrose in parallel. Colonies that were kanamycin-resistant and sucrose-sensitive were grown in plain LB for 2 days. Subsequently, cells were plated on methanol mineral medium plates supplemented with 6 % sucrose in serial dilution. Colonies were restreaked on LB with kanamycin and LB with 3 % sucrose in parallel. Kanamycin-sensitive, sucrose-resistant clones were screened for the successful deletion or integration of genes by colony PCR.

Preparation of cell-free extracts

P. denitrificans cultures were grown at 30 °C in mineral medium supplemented with various carbon sources. Cells were harvested at mid-exponential phase, resuspended in ice-cold MOPS/KOH buffer (100 mM, pH 7.2) and lyzed by sonication (MS-72, 40 %, 3 x 15 pulses). Cell debris was removed by centrifugation at 35 000 x g and 4 °C for 1 h. The total protein concentration of the cell-free extracts was determined with the Bradford assay (31) using bovine serum albumin (BSA) as standard. The catalytic activities of crotonyl-CoA carboxylase/reductase and isocitrate lyase were measured spectrophotometrically as described previously (3, 32).

Synthesis of crotonyl-CoA

Crotonyl-Coenzyme A was synthesized from its anhydride as described before (33).

Live-cell imaging

To monitor gene expression *in vivo*, cells were immobilized on 1% agarose pads and analyzed microscopically using an Axio Observer.Z1 (Zeiss) microscope equipped with a Plan Apochromat 100x/1.4 Oil Ph3 phase contrast objective, an ET-mCherry filter set (Chroma, USA) and a pco-edge sCMOS camera (PCO). Images were recorded with VisiView 3.3.0.6 (Visitron Systems, Germany) and processed with Fiji (34) and Adobe IllustratorCS5 (Adobe Systems, USA). For timelapse imaging, cells were transferred to a B04 CellASIC® ONIX2 microfluidic plate (Merck, Germany) coupled to a ONIX EV262 microfluidic platform (CellASIC, USA), cultivated at 30 °C under continuous medium flow (1 psi) and imaged at regular intervals using the microscope set-up described above. For automated data analysis, images were processed with Fiji (34) and BacStalk (10).

Heterologous production and purification of 6xHis-Icl

Competent *E. coli* BL21 cells were transformed with the expression plasmid pET16b_icl, and grown at 37 °C in Terrific Broth (23.6 g/L yeast extract, 11.8 g/L tryptone, 9.4 g/L K_2HPO_4, 2.2 g/L KH_2PO_4 and 4% (v/v) glycerol) supplemented with ampicillin. Gene expression was induced at OD_{600} = 0.8 by addition of 0.5 mM isopropylthio-galactopyranoside (IPTG). After additional growth at 18 °C for 12 h,

cells were harvested, resuspended in 3 volumes of buffer A (500 mM NaCl, 50 mM Tris-HCl, pH 7.9) containing 0.1 mg of DNase I and Protease Inhibitor Cocktail (Sigma-Aldrich, St. Louis, USA), and lyzed by sonication. Lysates were cleared by centrifugation at 42 000 x g and 4 °C for 45 min. The supernatant was applied onto a pre-equilibrated 1 mL Ni-Sepharose Fast Flow Column (HiTrap™, FF, GE Life Science, UK) and washed with buffer A. Proteins were eluted from the column by the addition of increasing concentrations of buffer B (500 mM NaCl, 50 mM Tris-HCl, 500 mM imidazole, pH7.9) followed by application onto a 5 mL HiTrap® Desalting Column (GE Life Science, UK) for desalting and buffer exchange to storage buffer (buffer A, 10 % glycerol). Protein concentration was determined using a NanoDrop® 2000 spectrometer (Thermo Scientific, USA) and purity was analyzed by SDS-PAGE according to (35).

Measurement of enzyme activities in cell-free extracts and purified protein

Ccr. Enzyme activity of crotonyl-CoA carboxylase/reductase was measured by following the consumption of NADPH spectrophotometrically as described earlier (3).

Icl. Enzyme activity of isocitrate lyase was measured by following the production of a phenylhydrazine-glyoxylate complex as described earlier (32). For the Icl inhibition assay with 3-nitropropionate (3-NPA), the compound was pre-equilibrated in 100 mM MOPS/KOH pH 7.2 oN. Purified isocitrate lyase was incubated in the reaction mixture containing 3-NPA at various concentrations at 30 °C for 10 min before the assay was started by addition of 2 mM D,L-isocitric acid.

Phylogenetic analysis

Sequences of twelve proteins (GapA; GyrA; RecA; RpoA; RpoB; TrpB; 30S ribosomal protein S2; 30S ribosomal protein S3; 30S ribosomal protein S12; 50S ribosomal protein L2; 50S ribosomal protein L3; 50S ribosomal protein L11) from the core proteome of 48 strains of *Paracoccus* were downloaded from the IMG database (36) and aligned using MUSCLE 3.8.31 (37). The alignments were concatenated and used to calculate a phylogenetic tree with MEGA 7.0.14 (38) using the maximum likelihood method with the Le-Gascuel substitution model and 100 bootstrap replicates. The resulting tree was visualized using iTOL (39).

Sequences of Ccr and Icl from 43 and 14 strains of *Paracoccus*, respectively, were downloaded from the IMG database and used to calculate maximum likelihood phylogenetic trees as described above.

References

1. Kornberg HL, Madsen NB. 1957. Synthesis of C4-dicarboxylic acids from acetate by a glyoxylate bypass of the tricarboxylic acid cycle. Biochim Biophys Acta 24:651-3.
2. Kornberg HL, Krebs HA. 1957. Synthesis of cell constituents from C2-units by a modified tricarboxylic acid cycle. Nature 179:988-91.
3. Erb TJ, Berg IA, Brecht V, Muller M, Fuchs G, Alber BE. 2007. Synthesis of C5-dicarboxylic acids from C2-units involving crotonyl-CoA carboxylase/reductase: the ethylmalonyl-CoA pathway. Proc Natl Acad Sci U S A 104:10631-6.
4. Erb TJ, Fuchs G, Alber BE. 2009. (2S)-Methylsuccinyl-CoA dehydrogenase closes the ethylmalonyl-CoA pathway for acetyl-CoA assimilation. Mol Microbiol 73:992-1008.
5. Erb TJ, Brecht V, Fuchs G, Muller M, Alber BE. 2009. Carboxylation mechanism and stereochemistry of crotonyl-CoA carboxylase/reductase, a carboxylating enoyl-thioester reductase. Proc Natl Acad Sci U S A 106:8871-6.
6. Claassen PAM, Vandenheuvel MHMJ, Zehnder AJB. 1987. Enzyme profiles of *Thiobacillus-versutus* after aerobic and denitrifying growth - regulation of isocitrate lyase. Archives of Microbiology 147:30-36.
7. Claassen PAM, Zehnder AJB. 1986. Isocitrate lyase activity in *Thiobacillus versutus* grown anaerobically on acetate and nitrate. Journal of General Microbiology 132:3179-3185.
8. Lee YV, Wahab HA, Choong YS. 2015. Potential inhibitors for isocitrate lyase of *Mycobacterium tuberculosis* and non-*M. tuberculosis*: a summary. Biomed Res Int 2015:895453.
9. Schloss JV, Cleland WW. 1982. Inhibition of isocitrate lyase by 3-nitropropionate, a reaction-intermediate analogue. Biochemistry 21:4420-7.
10. Hartmann R, van Teeseling MCF, Thanbichler M, Drescher K. 2018. BacStalk: a comprehensive and interactive image analysis software tool for bacterial cell biology. bioRxiv doi:10.1101/360230:360230.
11. Remus-Emsermann MN, Gisler P, Drissner D. 2016. MiniTn7-transposon delivery vectors for inducible or constitutive fluorescent protein expression in *Enterobacteriaceae*. FEMS Microbiol Lett 363.
12. Peyraud R, Schneider K, Kiefer P, Massou S, Vorholt JA, Portais JC. 2011. Genome-scale reconstruction and system level investigation of the metabolic network of *Methylobacterium extorquens* AM1. BMC Syst Biol 5:189.
13. Niebel B, Leupold S, Heinemann M. 2019. An upper limit on Gibbs energy dissipation governs cellular metabolism.
14. Nayak DD, Agashe D, Lee MC, Marx CJ. 2016. Selection maintains apparently degenerate metabolic pathways due to tradeoffs in using methylamine for carbon versus nitrogen. Curr Biol 26:1416-26.
15. Cruz AH, Brock M, Zambuzzi-Carvalho PF, Santos-Silva LK, Troian RF, Goes AM, Soares CM, Pereira M. 2011. Phosphorylation is the major mechanism regulating isocitrate lyase activity in *Paracoccidioides brasiliensis* yeast cells. FEBS J 278:2318-32.
16. Hoyt JC, Reeves HC. 1988. *In vivo* phosphorylation of isocitrate lyase from *Escherichia coli* D5H3G7. Biochem Biophys Res Commun 153:875-80.
17. Robertson EF, Reeves HC. 1989. Phosphorylation of isocitrate lyase in *Escherichia coli*. Biochimie 71:1065-70.
18. Murima P, Zimmermann M, Chopra T, Pojer F, Fonti G, Dal Peraro M, Alonso S, Sauer U, Pethe K, McKinney JD. 2016. A rheostat mechanism governs the bifurcation of carbon flux in *mycobacteria*. Nat Commun 7:12527.
19. Beijerinck M, Minkman D. 1910. Bildung und Verbrauch von Stickoxydul durch Bakterien. Zentbl Bakteriol Parasitenkd Infektionskr Hyg Abt II 25:30-63.
20. de Vries GE, Harms N, Hoogendijk J, Stouthamer AH. 1989. Isolation and characterization of *Paracoccus denitrificans* mutants with increased conjugation frequencies and pleiotropic loss of a (nGATCn) DNA-modifying property. Archives of Microbiology 152:52-57.
21. Hahnke SM, Moosmann P, Erb TJ, Strous M. 2014. An improved medium for the anaerobic growth of *Paracoccus denitrificans* Pd1222. Front Microbiol 5:18.
22. Peyraud R, Kiefer P, Christen P, Massou S, Portais JC, Vorholt JA. 2009. Demonstration of the ethylmalonyl-CoA pathway by using 13C metabolomics. Proc Natl Acad Sci U S A 106:4846-51.
23. Thoma S, Schobert M. 2009. An improved *Escherichia coli* donor strain for diparental mating. FEMS Microbiol Lett 294:127-32.

24. Peel D, Quayle JR. 1961. Microbial growth on C1 compounds. I. Isolation and characterization of *Pseudomonas* AM 1. Biochem J 81:465-9.
25. Sambrook J, Russel, D. W. 2001. Molecular cloning: A laboratory manual. Cold Spring Harbour Laboratory Press.
26. Schafer A, Tauch A, Jager W, Kalinowski J, Thierbach G, Puhler A. 1994. Small mobilizable multi-purpose cloning vectors derived from the *Escherichia coli* plasmids pK18 and pK19: selection of defined deletions in the chromosome of *Corynebacterium glutamicum*. Gene 145:69-73.
27. Drepper T, Eggert T, Circolone F, Heck A, Krauss U, Guterl JK, Wendorff M, Losi A, Gartner W, Jaeger KE. 2007. Reporter proteins for in vivo fluorescence without oxygen. Nat Biotechnol 25:443-5.
28. Shaner NC, Campbell RE, Steinbach PA, Giepmans BNG, Palmer AE, Tsien RY. 2004. Improved monomeric red, orange and yellow fluorescent proteins derived from *Discosoma* sp red fluorescent protein. Nature Biotechnology 22:1567-1572.
29. Rizzo MA, Springer GH, Granada B, Piston DW. 2004. An improved cyan fluorescent protein variant useful for FRET. Nat Biotechnol 22:445-9.
30. Thanbichler M, Iniesta AA, Shapiro L. 2007. A comprehensive set of plasmids for vanillate- and xylose-inducible gene expression in *Caulobacter crescentus*. Nucleic Acids Res 35:e137.
31. Bradford MM. 1976. A rapid and sensitive method for the quantitation of microgram quantities of protein utilizing the principle of protein-dye binding. Anal Biochem 72:248-54.
32. Brock M, Darley D, Textor S, Buckel W. 2001. 2-Methylisocitrate lyases from the bacterium *Escherichia coli* and the filamentous fungus *Aspergillus nidulans*: characterization and comparison of both enzymes. Eur J Biochem 268:3577-86.
33. Peter DM, Vogeli B, Cortina NS, Erb TJ. 2016. A chemo-enzymatic road map to the synthesis of coa esters. Molecules 21:517.
34. Schindelin J, Arganda-Carreras I, Frise E, Kaynig V, Longair M, Pietzsch T, Preibisch S, Rueden C, Saalfeld S, Schmid B, Tinevez JY, White DJ, Hartenstein V, Eliceiri K, Tomancak P, Cardona A. 2012. Fiji: an open-source platform for biological-image analysis. Nat Methods 9:676-82.
35. Laemmli UK. 1970. Cleavage of structural proteins during the assembly of the head of bacteriophage T4. Nature 227:680-5.
36. Markowitz VM, Chen IMA, Palaniappan K, Chu K, Szeto E, Grechkin Y, Ratner A, Jacob B, Huang JH, Williams P, Huntemann M, Anderson I, Mavromatis K, Ivanova NN, Kyrpides NC. 2012. IMG: the integrated microbial genomes database and comparative analysis system. Nucleic Acids Research 40:D115-D122.
37. Edgar RC. 2004. MUSCLE: multiple sequence alignment with high accuracy and high throughput. Nucleic Acids Res 32:1792-7.
38. Kumar S, Stecher G, Tamura K. 2016. MEGA7: Molecular evolutionary genetics analysis version 7.0 for bigger datasets. Molecular Biology and Evolution 33:1870-1874.
39. Letunic I, Bork P. 2016. Interactive tree of life (iTOL) v3: an online tool for the display and annotation of phylogenetic and other trees. Nucleic Acids Research 44:W242-W245.

559 # Tables

560 ***Table 1: Genes coding for enzymes of the EMCP and the GC in* Rhodobacter sphaeroides *2.4.1***
561 ***and* Escherichia coli *K-12, respectively, and their homologues identified in* P. denitrificans**
562 ***Pd1222.*** *Key enzymes of the two pathways are highlighted in bold. Missing enzyme homologues are*
563 *indicated by dashes.*

Enzyme		Gene name	Gene ID		
			R. sphaeroides 2.4.1	*E. coli* K-12	*P. denitrificans* Pd1222
EMCP	β-kethothiolase	*phaA*	RSP_ 0745	-	Pden_2026
	Acetoacetyl-CoA reductase	*phaB*	RSP_ 0747	-	Pden_2027
	Crotonyl-CoA carboxylase/reductase	***ccr***	**RSP_ 0960**	**-**	**Pden_3873**
	Ethylmalonyl-CoA/methylmalonyl-CoA epimerase	*epi*	RSP_ 0812	-	Pden_2178
	Ethylmalonyl-CoA mutase	*ecm*	RSP_ 0961	-	Pden_3875
	(*2S*)-methylsuccinyl-CoA dehydrogenase	*mcd*	RSP_ 1679	-	Pden_2840
	Mesaconyl-CoA hydratase	*mch*	RSP_ 0973	-	Pden_0566
	β-methylmalyl-CoA/L-malyl-CoA lyase	*mcl-1*	RSP_ 1771	-	Pden_0799
	(*S*)-malyl-CoA thioesterase	*mcl-2*	RSP_0970	-	Pden_0563
	Propionyl-CoA carboxylase	*pccAB*	RSP_ 2191/2189	-	Pden_3684/3688
	Ethylmalonyl-CoA/methylmalonyl-CoA epimerase	*epi*	RSP_ 0812	-	Pden_2178
	(*2R*)-methylmalonyl-CoA mutase	*mcm*	RSP_ 2912	-	Pden_3681
GC	**Isocitrate lyase**	***aceA***	**-**	**C5Y66_09370**	**Pden_1363**
	Malate synthase	*aceB*	-	C5Y66_09365	Pden_1364

564

565 ***Table 2: Strains used in this study***

Strain	Genotype or relevant features	Reference
E. coli TOP 10	cloning strain	Invitrogen, USA
E. coli DH5α	cloning strain	Thermo Fisher Scientific, USA
E. coli BL21	protein expression	Thermo Fisher Scientific, USA
E. coli ST18	mating strain	(23)
M. extorquens AM1	wild type	(24)
P. denitrificans DSM413	wild type	(19)
P. denitrificans Pd1222	increased conjugation frequency	(20)
P. denitrificans DSM413 Δ*ccr* (TJE-KK5)	Δ*ccr*	This work
P. denitrificans DSM413 Δ*icl* (TJE-KK6)	Δ*icl*	This work
P. denitrificans Pd1222 *ccr::ccr-mCherry icl::icl-cerulean* (TJE-KK14)	*ccr::ccr-mCherry icl::icl-cerulean*	This work
P. denitrificans Pd1222 *ccr::ccr-mCherry* (TJE-KK13)	*ccr::ccr-mCherry*	This work
P. denitrificans Pd1222 *icl::icl-mCherry* (TJE-KK10)	*icl::icl-mCherry*	This work

566

567 ***Table 3: Oligonucleotides used for plasmid construction and mutant verification in this study***

Oligonucleotide	Sequence	Purpose
NdeI_pKK21-f	TATATCATATGCCCCGGCCCCGGCGCATG	Generation of pTE1624
pKK21-r	TATATCCTAGGGCGGCGCCCCGCCTCCAGCGCGTC	
mCherry-f	TATATCCTAGGGCAGGGAGTGCGGCCGGCAG	
NdeI_mCherry-r	TATATCATATGTCACTTGTACAGCTCGTCCATG	
NdeI_pSYNiclXicIds-f	TATACATATGTCTAGAGGGCCGACAGGATTCGGCC	Generation of

HindIII_pSYNccrxccrds-r	TATATAAGCTTGCCGCTGCCGGCCGCACTCCCTGC	pTE1625
HindIII_cerulean-f	TATATAAGCTTATGGTGAGCAAGGGCGAGGAGC	
NdeI_cerulean-r	TATATCATATGTTACTTGTACAGCTCGTCCATGCCGAG	
NdeI_icl-f	TATACATATGAGCAGAAAGACTTTTTCGGAAATC	Generation of
HindIII_icl-r	TATAAAGCTTCTATTCGGCGGCGAACTGGTTCATGGTG	pTE1614
Pden_3873_ds-f	GGTCAGGCGCTTGTATTGGCCGAACATGTAG	Verification of
Pden_3873_ups-r	GCGAAAGCGGCATCGCCGTGGTGCGGATGAATTAC	TJE-KK5
Pden_1363_ds-f2	CATCCATTCATAGGCGGTGACCACCAGGCCC	Verification
Pden_1363_ups-r	GCTGGGACTATATCTTCAGCTATATCAAGAC	of TJE-KK6
Pden_1363_ds-f2	CATCCATTCATAGGCGGTGACCACCAGGCCC	
iclmCherryiclds_seq-f	CAGCATTGCCGAGGCCGACTACCCGGAC	Verification of
Pden_1363_ds-f	GACGAGCGCCGTGGTGAGTCTCAGCATGATGG	TJE-KK10
Pden_1363_ups-r	GCTGGGACTATATCTTCAGCTATATCAAGAC	
NdeI mCherry-r	TATATCATATGTCACTTGTACAGCTCGTCCATG	
Pden_3873_ups-r	GCGAAAGCGGCATCGCCGTGGTGCGGATGAATTAC	Verification
3'-ccr-f	CGCAGGCGCATCTGAAGATGC	of TJE-KK13
Pden_3873_ds-f	GGTCAGGCGCTTGTATTGGCCGAACATGTAG	
Pden_1363_ds-f2	CATCCATTCATAGGCGGTGACCACCAGGCCC	Verification of
Pden_1363_ups-r	GCTGGGACTATATCTTCAGCTATATCAAGAC	TJE-KK14
HindIII_cerulean-f	TATATAAGCTTATGGTGAGCAAGGGCGAGGAGC	

568

Figures

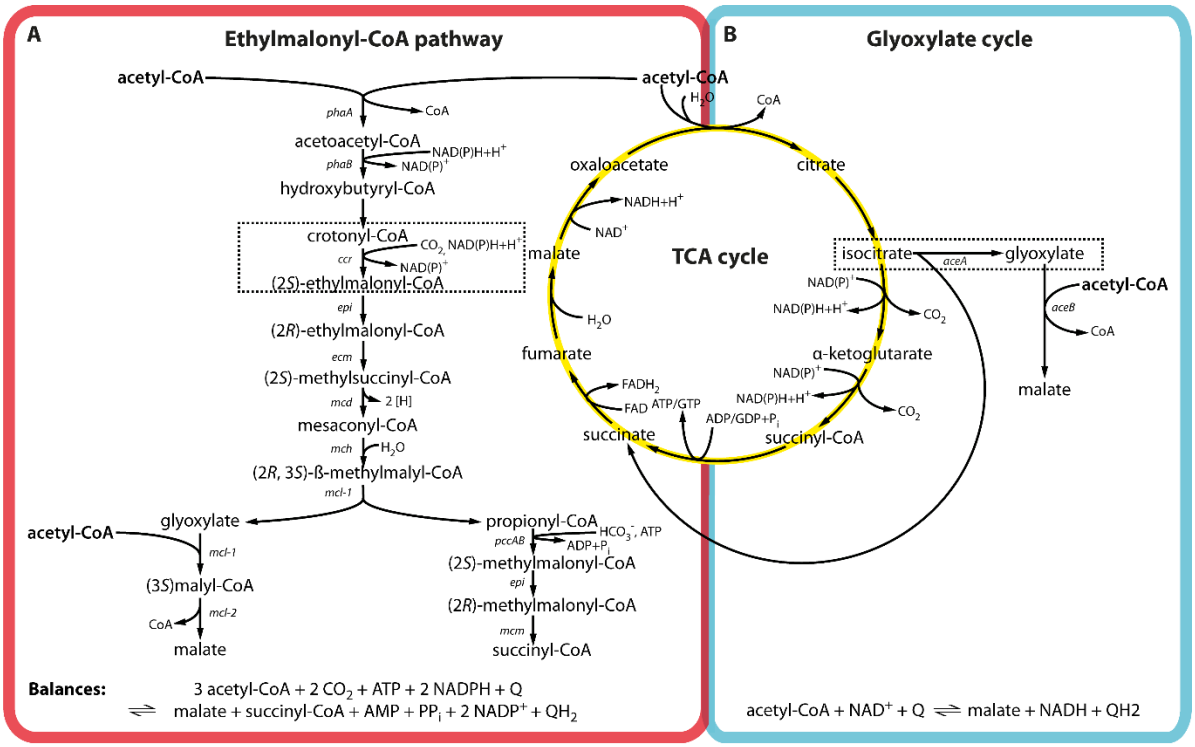

Figure 1: The fate of acetyl-CoA in anabolism and catabolism. *Acetyl-CoA is either oxidized to CO_2 in the tricarboxylic acid cycle (TCA) to generate reducing equivalents and ATP/GTP, or assimilated into biomass. Two acetyl-CoA assimilation pathways are present in bacteria, the ethylmalonyl-CoA pathway* ***(A)*** *and the glyoxylate cycle* ***(B)****. Reaction balances of the individual pathways are shown on the bottom. Note that the activation of acetate to acetyl-CoA requires the hydrolysis of one ATP into AMP and PP_i (not included in balance). Key reactions of the individual pathways are highlighted in dashed boxes. Genes encoding the individual enzymes of the EMCP and GC are named following the nomenclature established for* Rhodobacter sphaeroides *2.4.1 and* Escherichia coli *K-12, respectively. The corresponding enzyme names and open reading frames in* P. denitrificans *are listed in Table 1.*

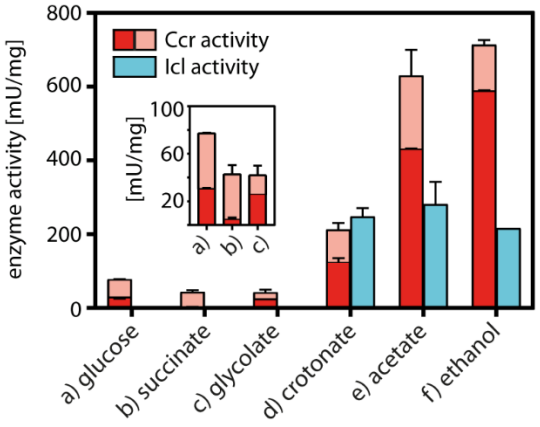

Figure 2: Ccr and Icl enzyme activities in cell-free extracts of* P. denitrificans *grown on different carbon sources. *Ccr activity is given as combined activity of reduction and reductive carboxylation of crotonyl-CoA, quantified in the absence (light red) and presence of $NaHCO_3$ (dark red), respectively. Error bars indicate standard deviation.*

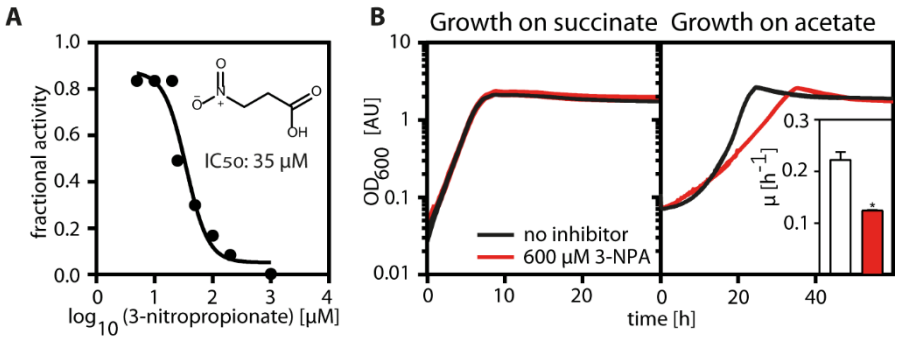

Figure 3: Inhibition of* P. denitrificans *Icl by 3-NPA in vitro (A) and in vivo (B). *(A) Recombinant His$_6$-tagged Icl was pre-incubated at 30°C for 10 min with increasing concentrations of 3-NPA before activity measurements. The fractional activity of Icl is plotted against the log$_{10}$ of the 3-NPA concentration. The apparent IC50 was determined using the log(inhibitor) vs. response function of GraphPad Prism7. (B) Growth of* P. denitrificans *on succinate and acetate in the absence (black line) and presence (red line) of 600 µM 3-NPA. The growth rates on acetate are shown in the inset. Growth on acetate is significantly inhibited by 3-NPA ($p < 0.5$ as determined by an unpaired t-test using GraphPad Prism7). Error bars indicate standard deviation.*

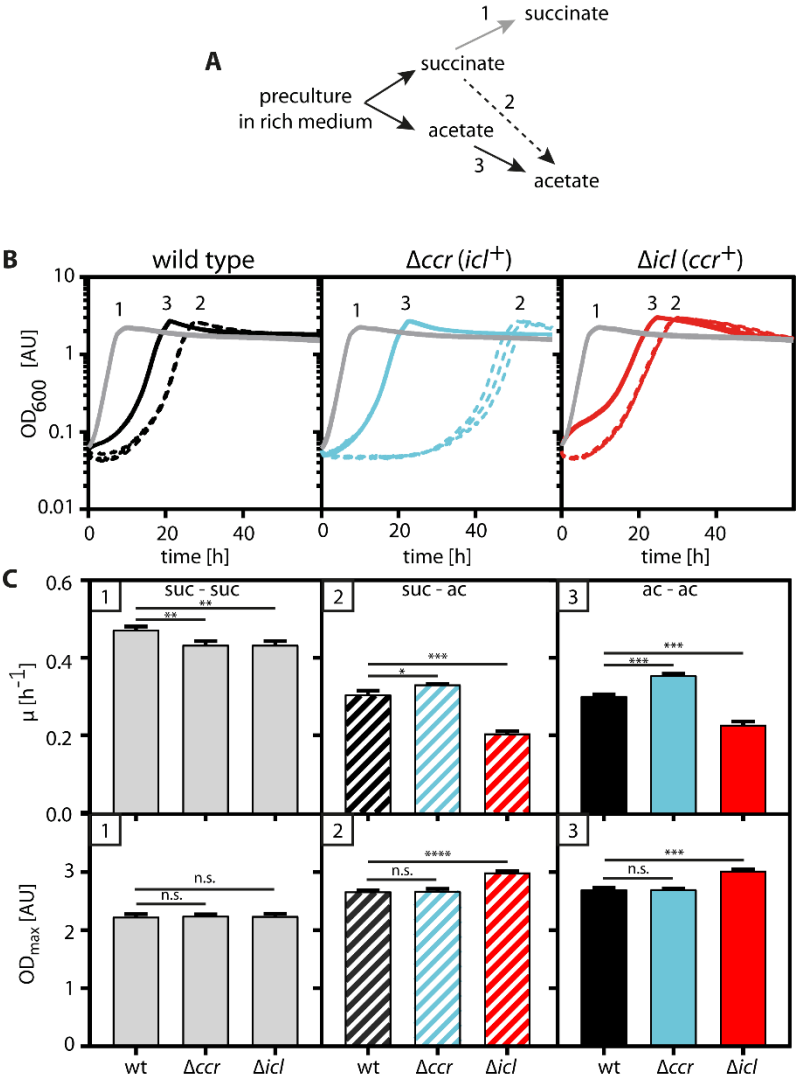

***Figure 4: Phenotypic characterization of* Δccr *and* Δicl.** *(A) Inoculation scheme. (B) Growth behavior of wild type,* Δccr *and* Δicl P. denitrificans *on succinate (grey lines; 1), after a switch from succinate to acetate (dashed lines; 2), or from acetate to acetate (solid lines; 3). The curves show*

*independently grown triplicates, in some cases the lines overlap. (C) Growth rates and maximum optical densities calculated from the curves shown in (B). Error bars indicate the standard deviation. Asterisks mark the level of significance of growth rate or maximal optical density between wild type and the individual mutants as determined by t-test with the number of asterisks indicating the decimal place of p (e.g. *** $p < 5 \times 10^{-3}$; n.s.: not significant). suc: succinate, ac: acetate.*

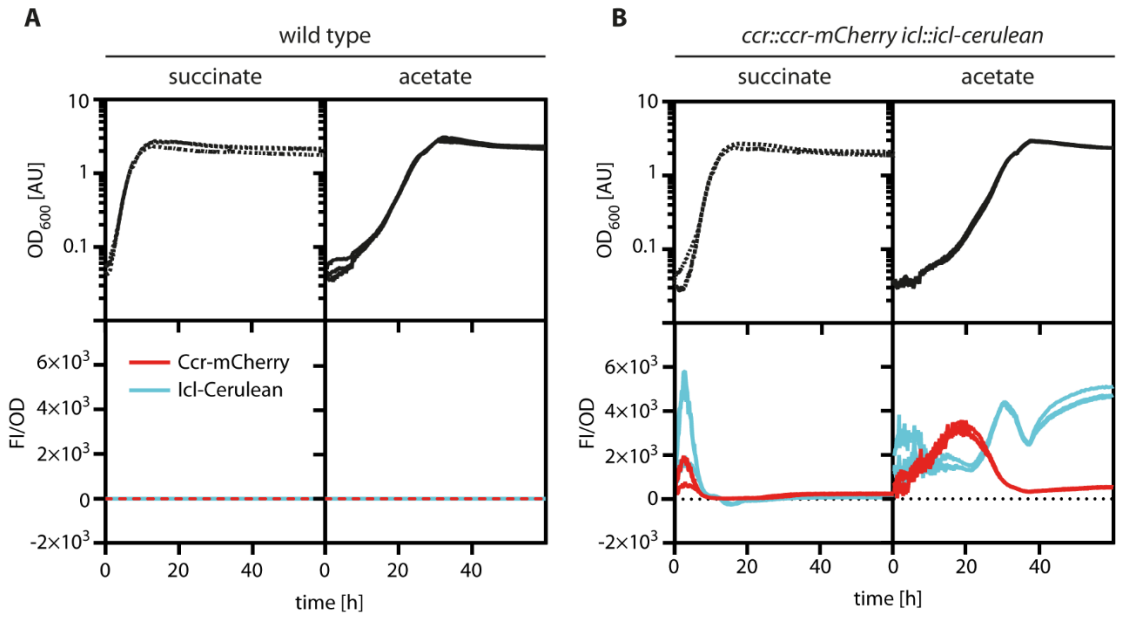

Figure 5: Expression of Ccr and Icl in* P. denitrificans *during growth on succinate and acetate. *The optical density (OD_{600}) and fluorescence intensity (FI) of the* P. denitrificans *wild type (A) and* ccr:ccr-mCherry icl::icl-cerulean *strain (B) were monitored during growth on succinate and acetate using a 96-well plate reader. Fluorescence was normalized to OD and corrected by the background signal of the wild type. The Ccr-mCherry level is shown in red and the Icl-Cerulean level is shown in cyan. Growth curves and fluorescent measurements are shown in triplicates, in some cases the lines overlap.*

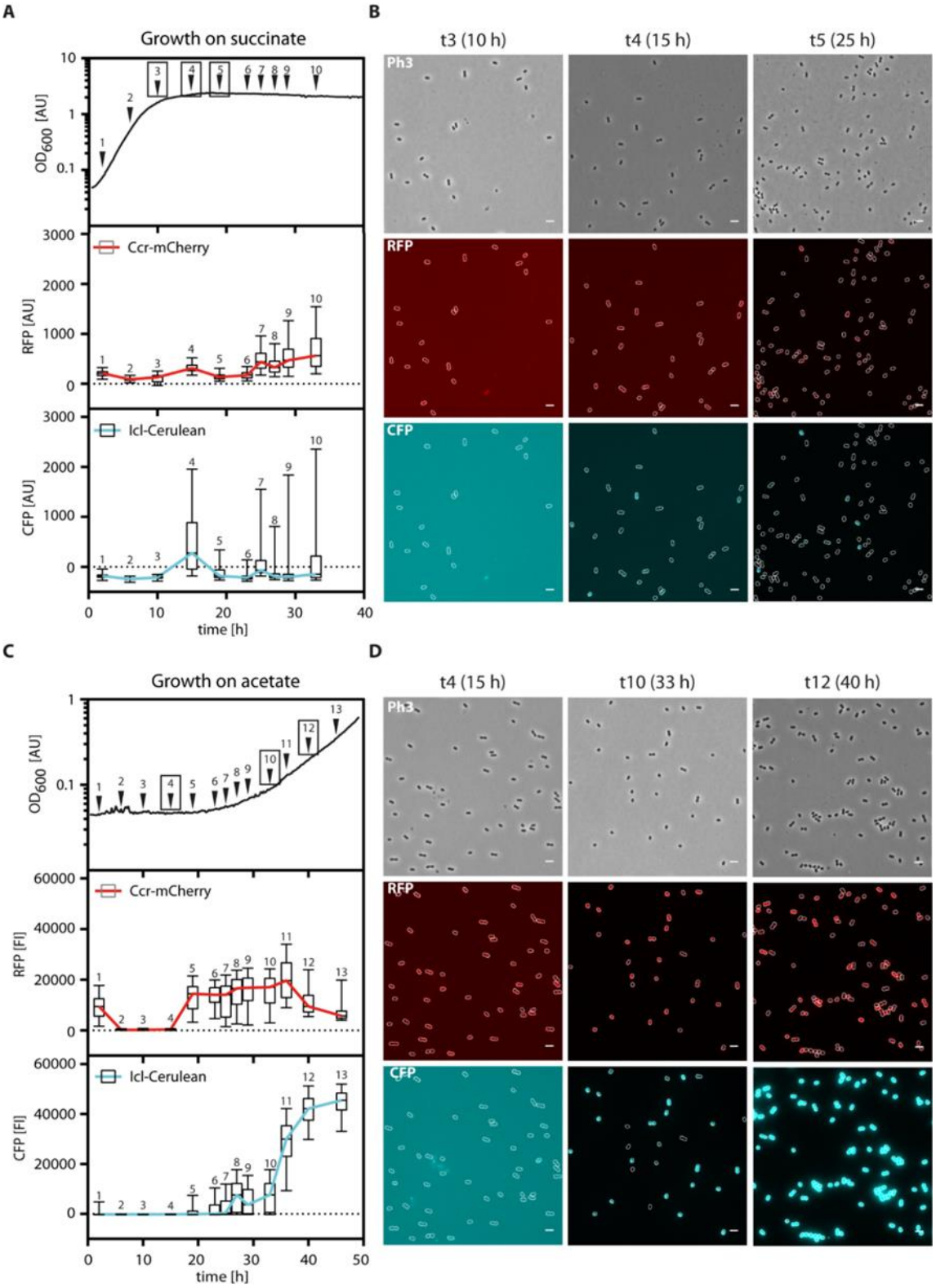

***Figure 6: Fluorescence of* P. denitrificans ccr::ccr-mCherry icl::icl-cerulean *during growth on succinate (A, B) and acetate (C, D)**. At the indicated time points, the cultures were sampled and analyzed microscopically. Images were subjected to automated analysis using BacStalk (10). (A) and (C) Distribution of cellular fluorescence intensities (n=450 cells per time point) shown as box plots. The values were corrected for the background fluorescence of the wild type. The margins of the boxes encompass the 25th to 75th percentiles, the lines indicate the median, and the whiskers extend to the 5th and 95th percentile, respectively. The colored lines connect the medians. (B) and (D) Representative microscopy images. Ph3, phase contrast; RFP, mCherry channel (overlaid with Ph3), CFP, Cerulean channel (overlaid with Ph3).*

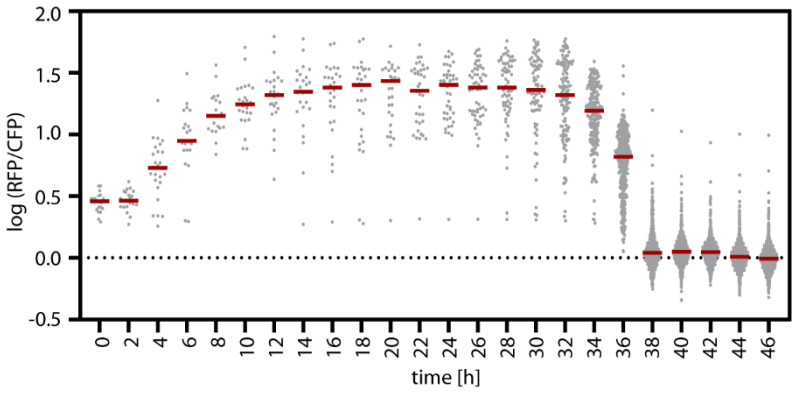

Figure 7: Comparison of Ccr-mCherry (RFP) to Icl-Cerulean (CFP) fluorescence in single cells over time*. Succinate-grown cells of the strain* P. denitrificans ccr::ccr-mCherry icl::icl-cerulean *were immobilized in a microfluidic system with a continuous flow of acetate minimal medium. Cell growth and fluorescence intensities were tracked by time-lapse fluorescence microscopy, observing the same field of view for 46 hours. The fluorescence intensities of individual cells, determined via automated image analysis (11), are plotted as the logarithmic ratio of the RFP and CFP intensities. Grey points represent the values of individual cells. The red lines mark the medians of the sampled populations.*

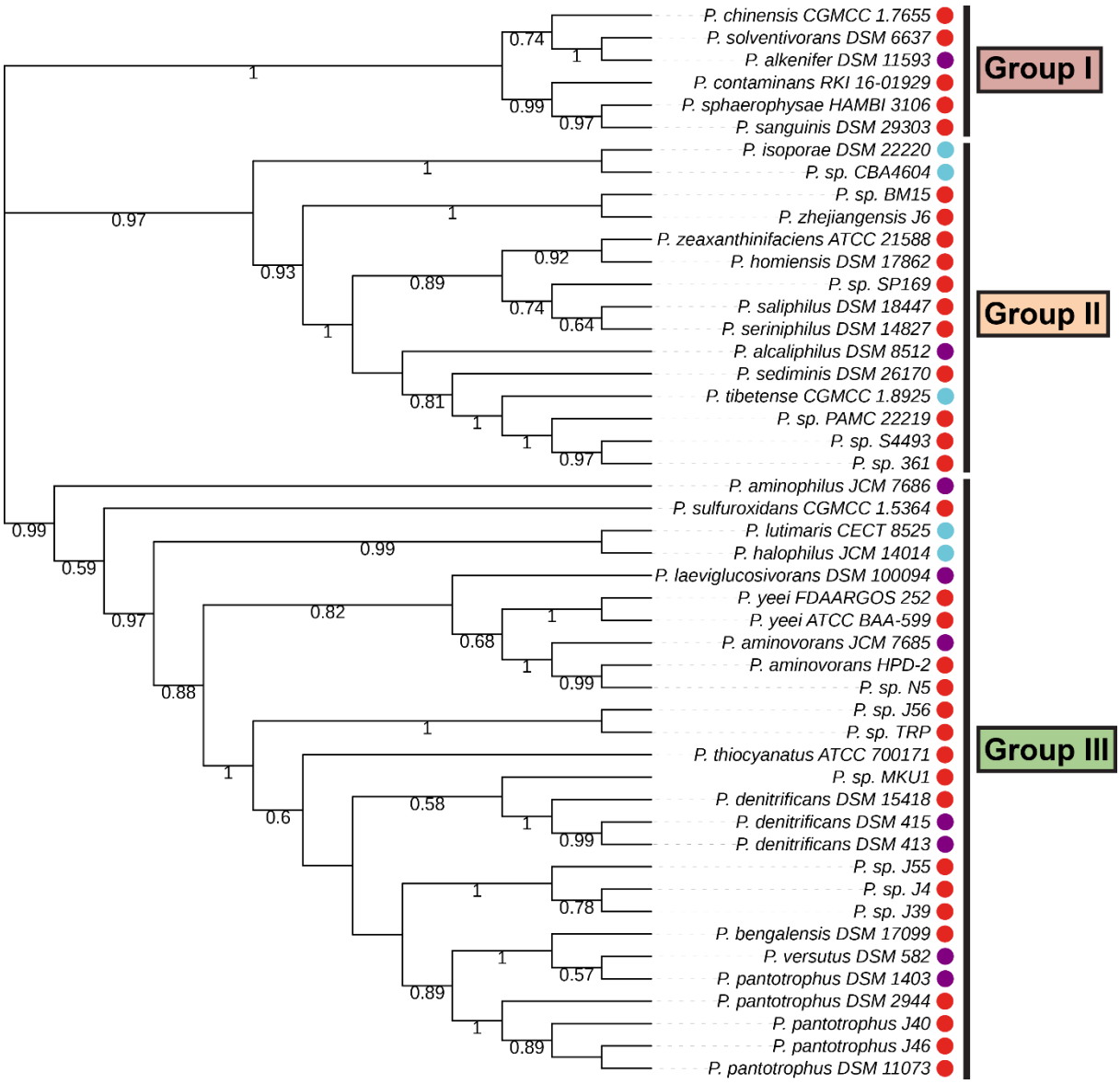

Figure 8: Maximum likelihood phylogenetic tree of* Paracoccus *strains. *The phylogenetic tree is based on the concatenated alignments of twelve protein sequences from 48* Paracoccus *strains. Bootstrap values ≥ 0.5 are given on the respective nodes; calculated branch lengths of the tree are ignored for the sake of easier visualization. Presence of Ccr is marked with a red dot, presence of Icl is marked with a blue dot, and presence of both enzymes is marked with a purple dot. The 48 strains are clustered in three distinct groups.*

Supplementary Information

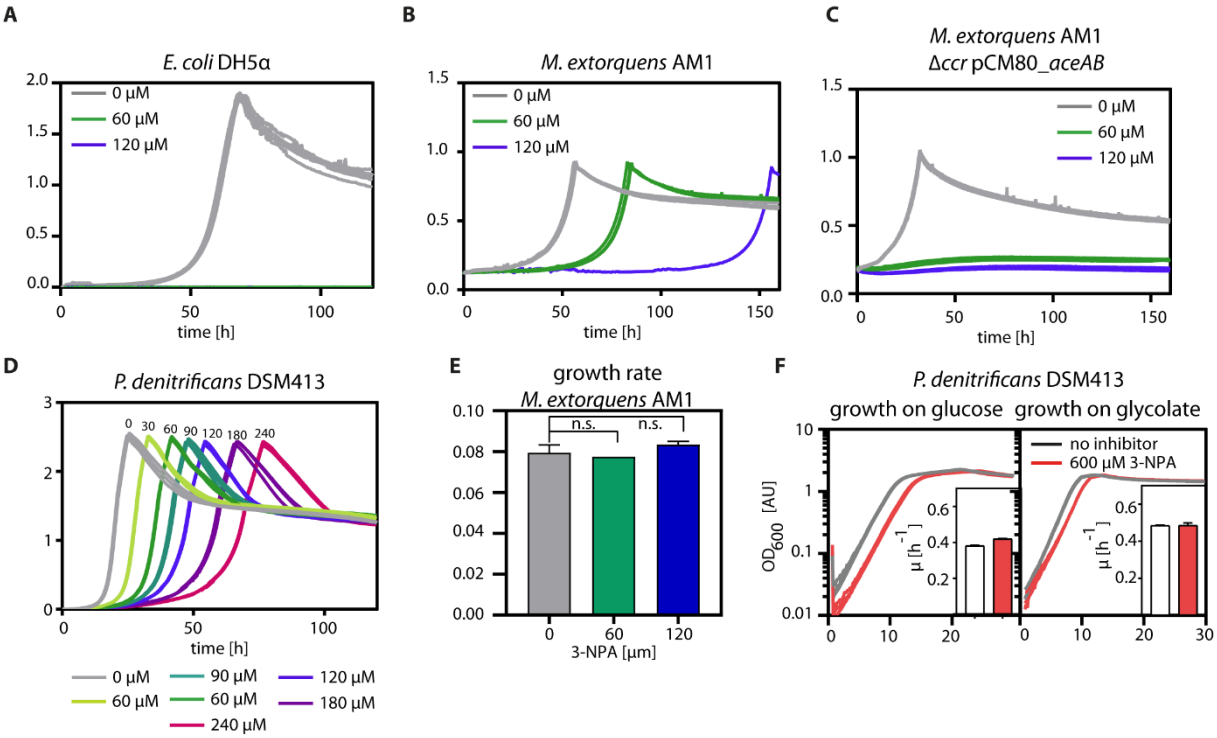

Figure S 1: Testing 3-NPA as suitable compound for the inhibition of Icl in* P. denitrificans *in vivo. *3-NPA was added to acetate minimal medium inoculated with* E. coli *DH5α (A),* M. extorquens *AM1 (B),* M. extorquens *AM1 lacking* ccr *but heterologously expressing the glyoxylate shunt of* E. coli, *and* P. denitrificans *DSM413 (D). (E) Growth rates corresponding to the growth curves in (B). Despite an extension of the lag phase, the growth rate of* M. extorquens *AM1 was not affected by the presence of 3-NPA. n.s.= not significant (F) Growth curves of* P. denitrificans *DSM413 on substrates, which do not require acetyl-CoA assimilation, in the absence and presence of 3-NPA with the corresponding growth rates. Error bars indicate standard deviation.*

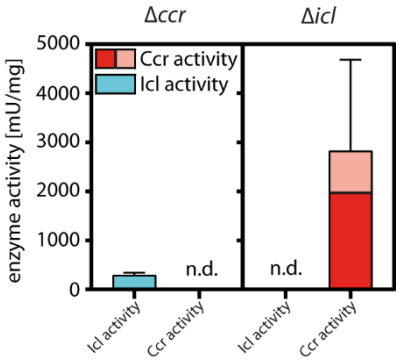

Figure S 2: Enzyme activites in* ccr *and* icl *deletion strains. *To confirm the absence of Ccr and Icl in the respective single-deletion backgrounds, enzyme activities were determined in cell-free extracts of the deletion strains grown to mid-exponential phase in acetate minimal medium. n.d.: not detectable. Dark red: Ccr activity with concomitant carboxylation. Light red: Ccr activity independent of carboxylation. Error bars indicate standard deviation.*

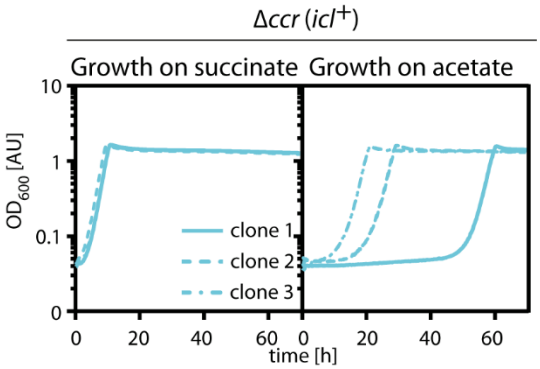

Figure S 3: Growth of individual clones of strain* P. denitrificans Δccr *on acetate and succinate. *Cells were grown in rich medium, washed and shifted to either acetate or succinate minimal medium. While all clones exhibited the same growth behavior on succinate, they displayed different lag phases during growth on acetate. The genotypes of all clones were confirmed by colony PCR after completion of the experiment.*

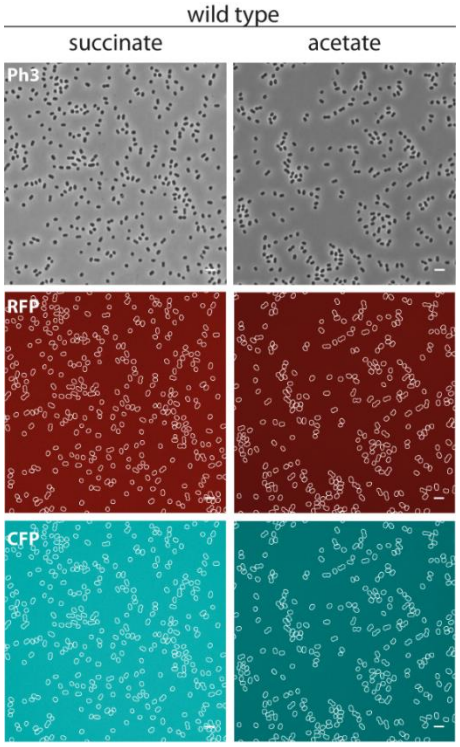

Figure S 4: Fluorescence of the* P. denitrificans *wild type. *Cells were grown on succinate and on acetate and analyzed microscopically to exclude the possibility that fluorescence detected in the analysis of* P. denitrificans ccr::ccr-mCherry icl::icl-cerulean *stemmed from autofluorescence of* P. denitrificans*. Scale bar: 3 µm.*

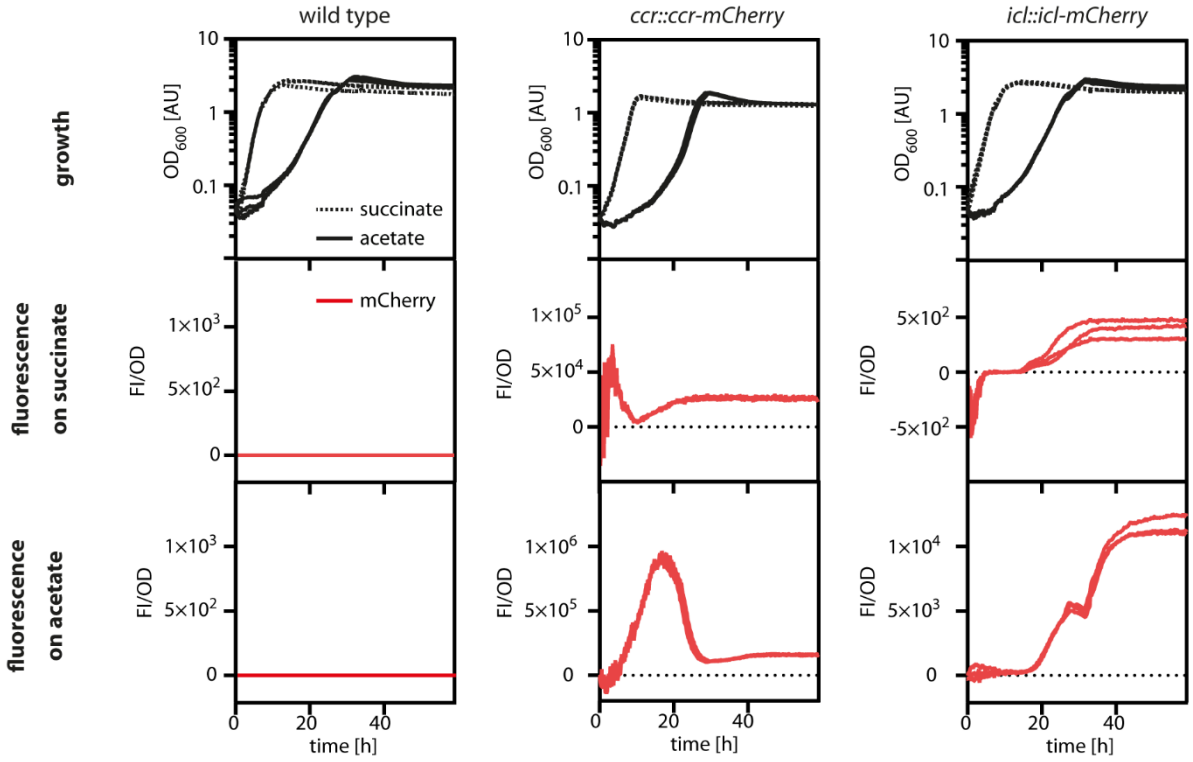

Figure S 5: Expression of Ccr-mCherry and Icl-mCherry in* P. denitrificans *single-reporter strains during growth on succinate and acetate. *Succinate and acetate cultures were started from washed succinate-grown pre-cultures. Growth curves and fluorescent measurements are shown in triplicates, in some cases the lines overlap. Fluorescence measurements of the individual strains were performed with different gain adjustments. Therefore, the absolute fluorescence intensity values cannot be compared between the different strains.*

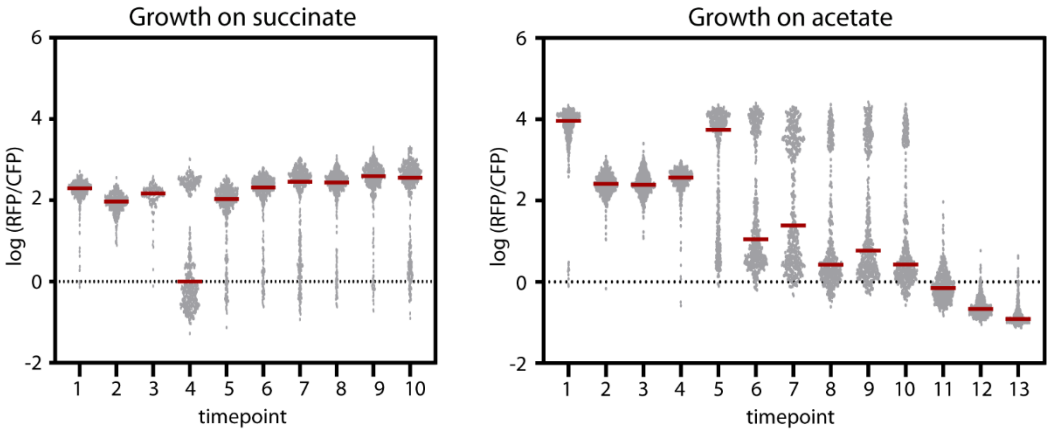

675

676 ***Figure S 6: Comparison of Ccr-mCherry (RFP) to Icl-Cerulean (CFP) fluorescence.*** *RFP and CFP*
677 *intensities of the strain* P. denitrificans ccr::ccr-mCherry icl::icl-cerulean *grown on succinate and*
678 *acetate (growth and individual fluorescence intensities shown in Figure 6) are plotted as logarithmic*
679 *ratios. Grey points represent the values of individual cells. The red lines mark the medians of the*
680 *sampled populations.*

681

682

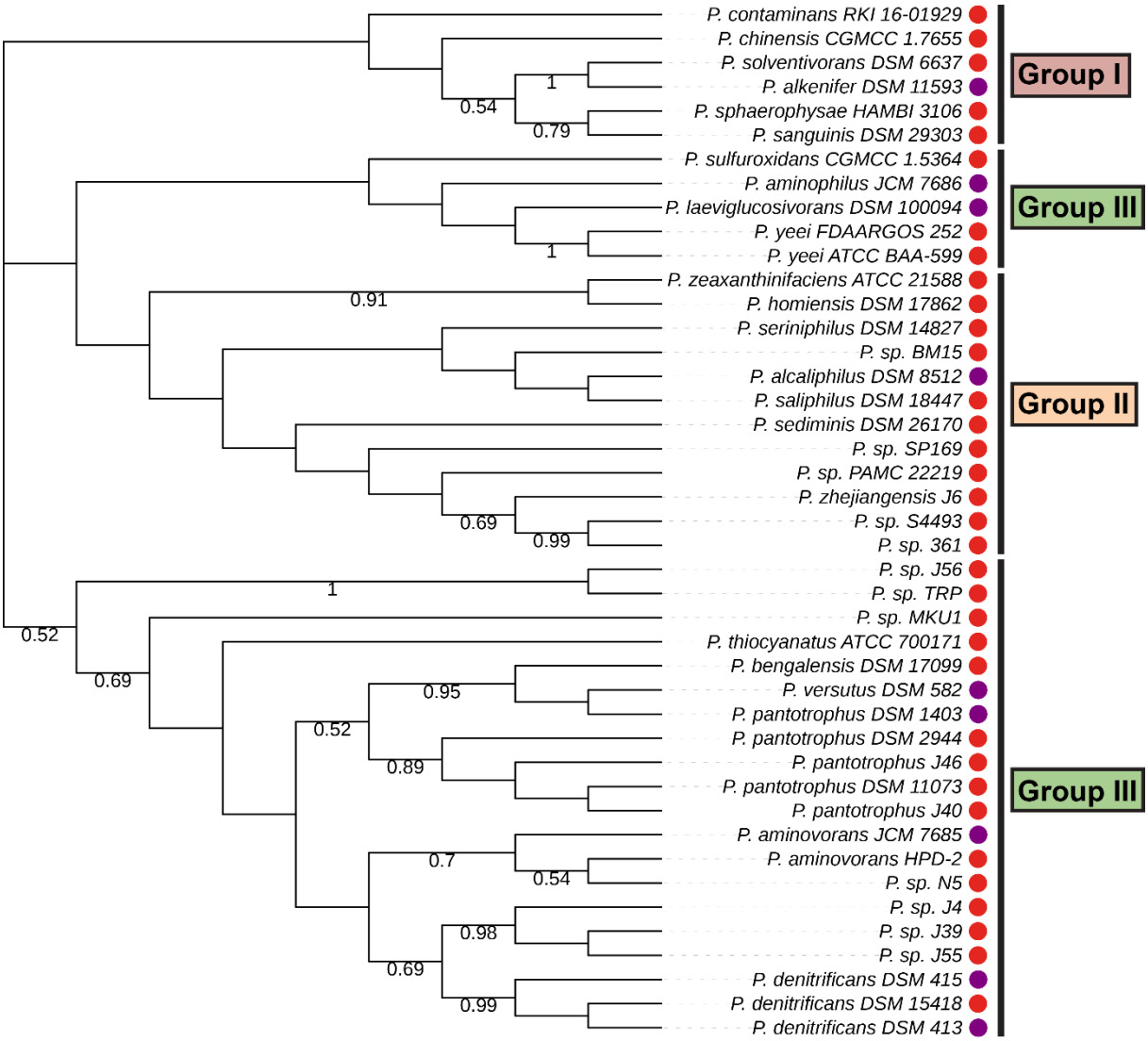

683

Figure S 7: Maximum likelihood phylogenetic tree of Ccr sequences. *The phylogenetic tree is based on Ccr sequences from 43* Paracoccus *strains. Bootstrap values ≥ 0.5 are given on the respective nodes; calculated branch lengths of the tree are ignored for the sake of easier visualization. Presence of Ccr is marked with a red dot, and presence of both Ccr and Icl is marked with a purple dot. The clustering of the 43 strains is largely similar to the phylogeny shown in Figure 8.*

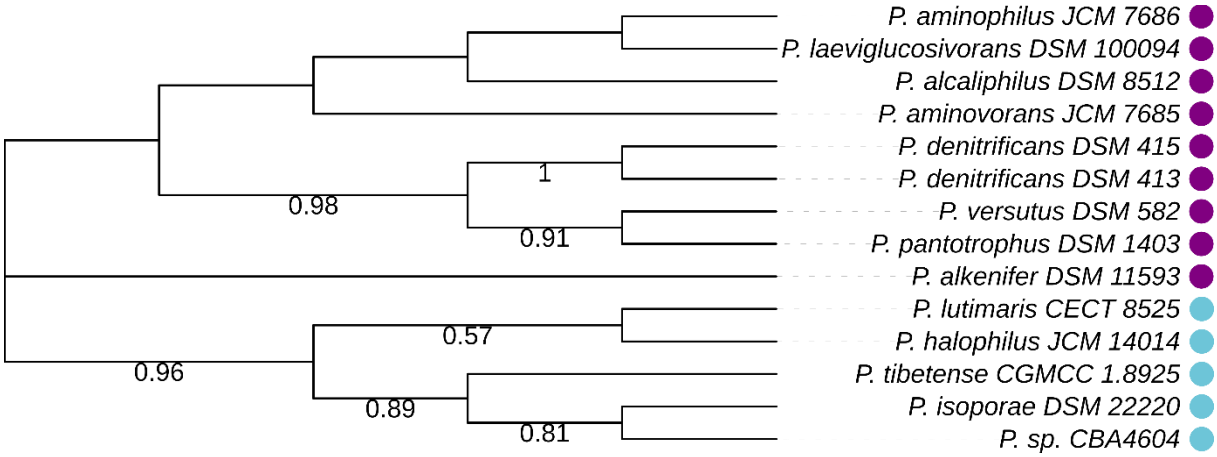

Figure S 8: Maximum likelihood phylogenetic tree of Icl sequences. *The phylogenetic tree is based on Icl sequences from 14* Paracoccus *strains. Bootstrap values ≥ 0.5 are given on the respective nodes; calculated branch lengths of the tree are ignored for the sake of easier visualization. Presence of Icl is marked with a blue dot, and presence of both Ccr and Icl is marked with a purple dot. Note that the Icl-positive strains of* Paracoccus *can be found in all three phylogenetic groups of the genus (compare Figure 8).*

Video S 1: Fluorescence of* P. denitrificans ccr::ccr-mCherry icl::icl-cerulean *during growth on acetate after switch from succinat*e. Cells were grown in succinate, trapped in a microfluidic device, and continuously flushed with acetate minimal medium. Images were taken every 2 h; time points are indicated on the individual frames of the video. Scale bar: 3 µm.***

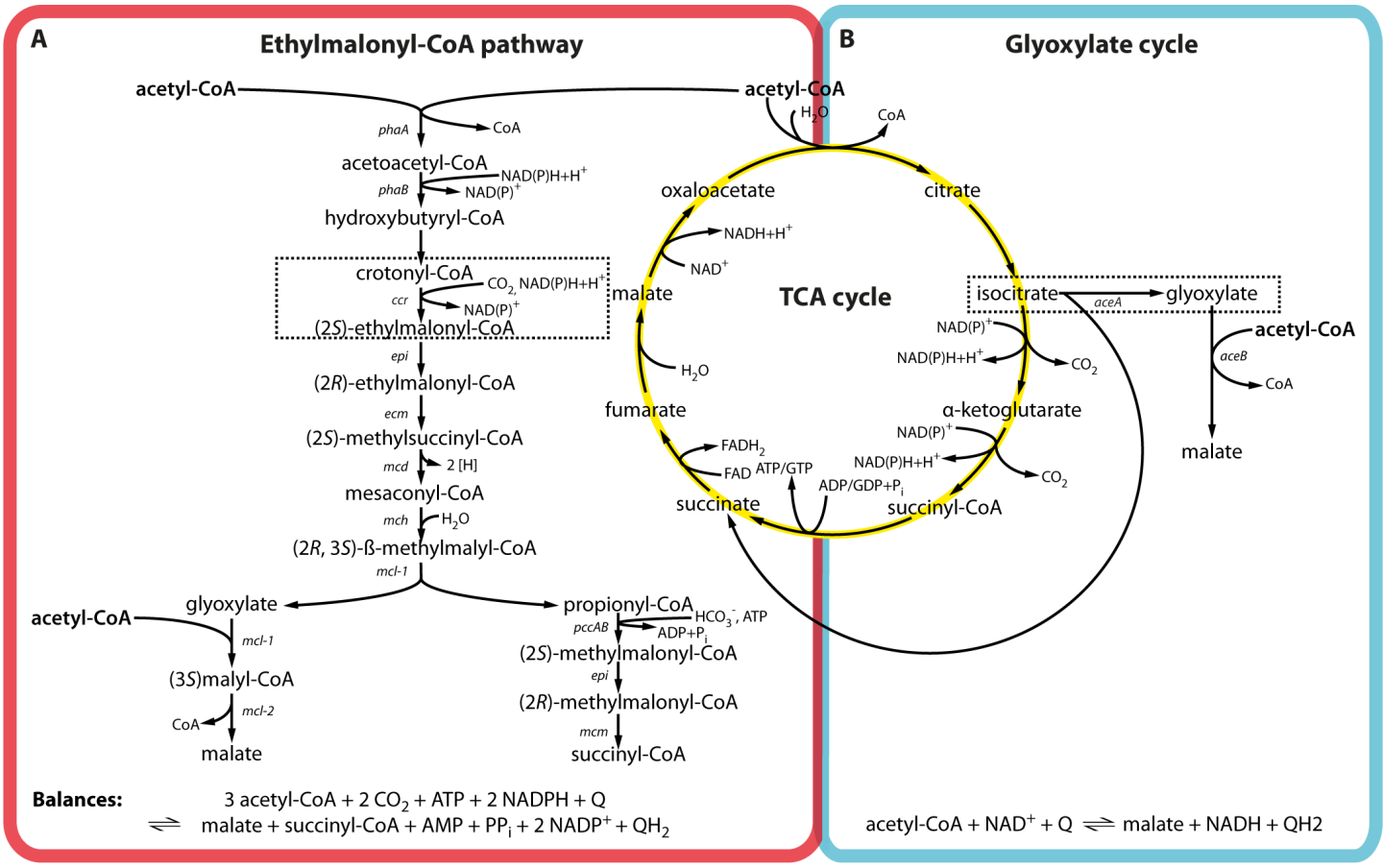
A
Ethylmalonyl-CoA pathway
acetyl-CoA
acetyl-CoA
phaA
CoA
acetoacetyl-CoA
NAD(P)H+H+
phaB
NAD(P)+
hydroxybutyryl-CoA
crotonyl-CoA
CO2, NAD(P)H+H+
ccr
NAD(P)+
(2S)-ethylmalonyl-CoA
epi
(2R)-ethylmalonyl-CoA
ecm
(2S)-methylsuccinyl-CoA
mcd
2 [H]
mesaconyl-CoA
mch
H2O
(2R, 3S)-ß-methylmalyl-CoA
mcl-1
acetyl-CoA
glyoxylate
mcl-1
(3S)malyl-CoA
CoA
mcl-2
malate
propionyl-CoA
HCO3-, ATP
pccAB
ADP+Pi
(2S)-methylmalonyl-CoA
epi
(2R)-methylmalonyl-CoA
mcm
succinyl-CoA
Balances:
3 acetyl-CoA + 2 CO2 + ATP + 2 NADPH + Q
malate + succinyl-CoA + AMP + PPi + 2 NADP+ + QH2
B
Glyoxylate cycle
acetyl-CoA
H2O
CoA
oxaloacetate
citrate
NADH+H+
NAD+
malate
TCA cycle
isocitrate
aceA
glyoxylate
NAD(P)+
NAD(P)H+H+
CO2
acetyl-CoA
aceB
CoA
H2O
fumarate
α-ketoglutarate
malate
NAD(P)+
FADH2
FAD
ATP/GTP
NAD(P)H+H+
CO2
ADP/GDP+Pi
succinate
succinyl-CoA
acetyl-CoA + NAD+ + Q malate + NADH + QH2

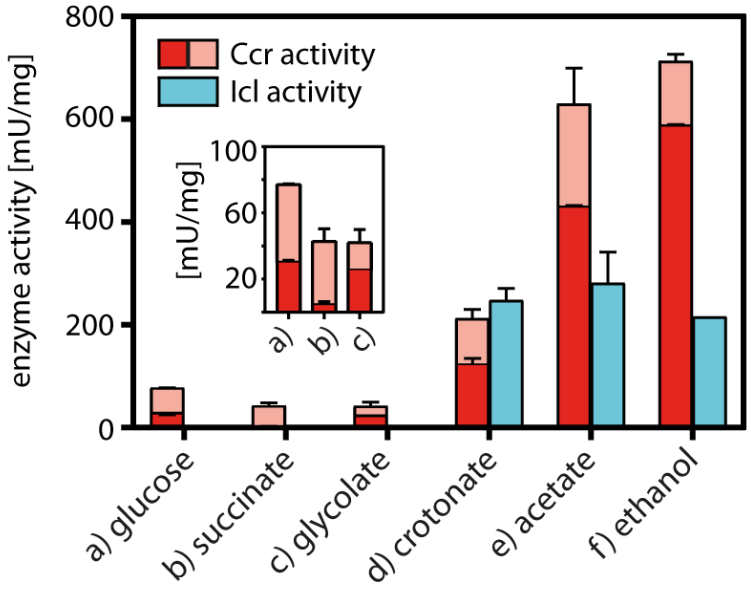
800
600
400
200
0
enzyme activity [mU/mg]
Ccr activity
Icl activity
100
60
20
[mU/mg]
a)
b)
c)
a) glucose
b) succinate
c) glycolate
d) crotonate
e) acetate
f) ethanol

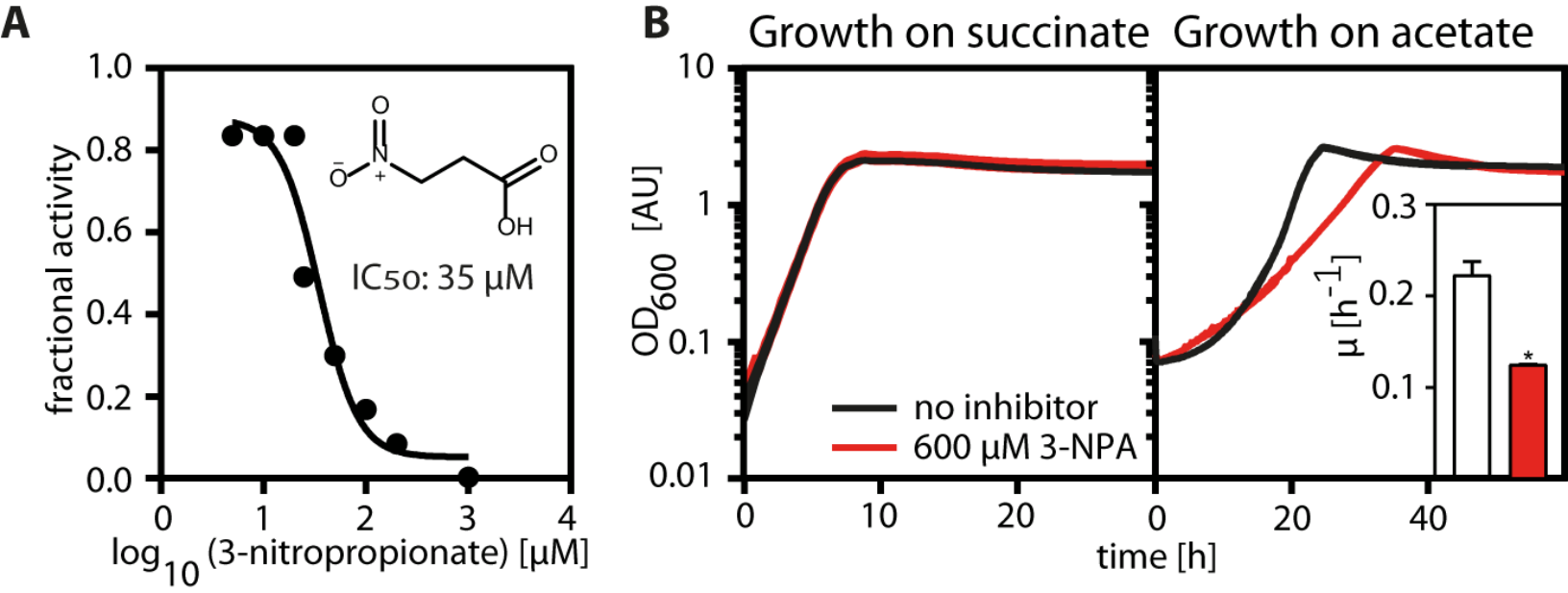
A
fractional activity
1.0
0.8
0.6
0.4
0.2
0.0
0
1
2
3
4
log10 (3-nitropropionate) [µM]
IC50: 35 µM
B
Growth on succinate
Growth on acetate
OD600 [AU]
10
1
0.1
0.01
no inhibitor
600 µM 3-NPA
0
10
20
0
20
40
time [h]
µ [h-1]
0.3
0.2
0.1
*

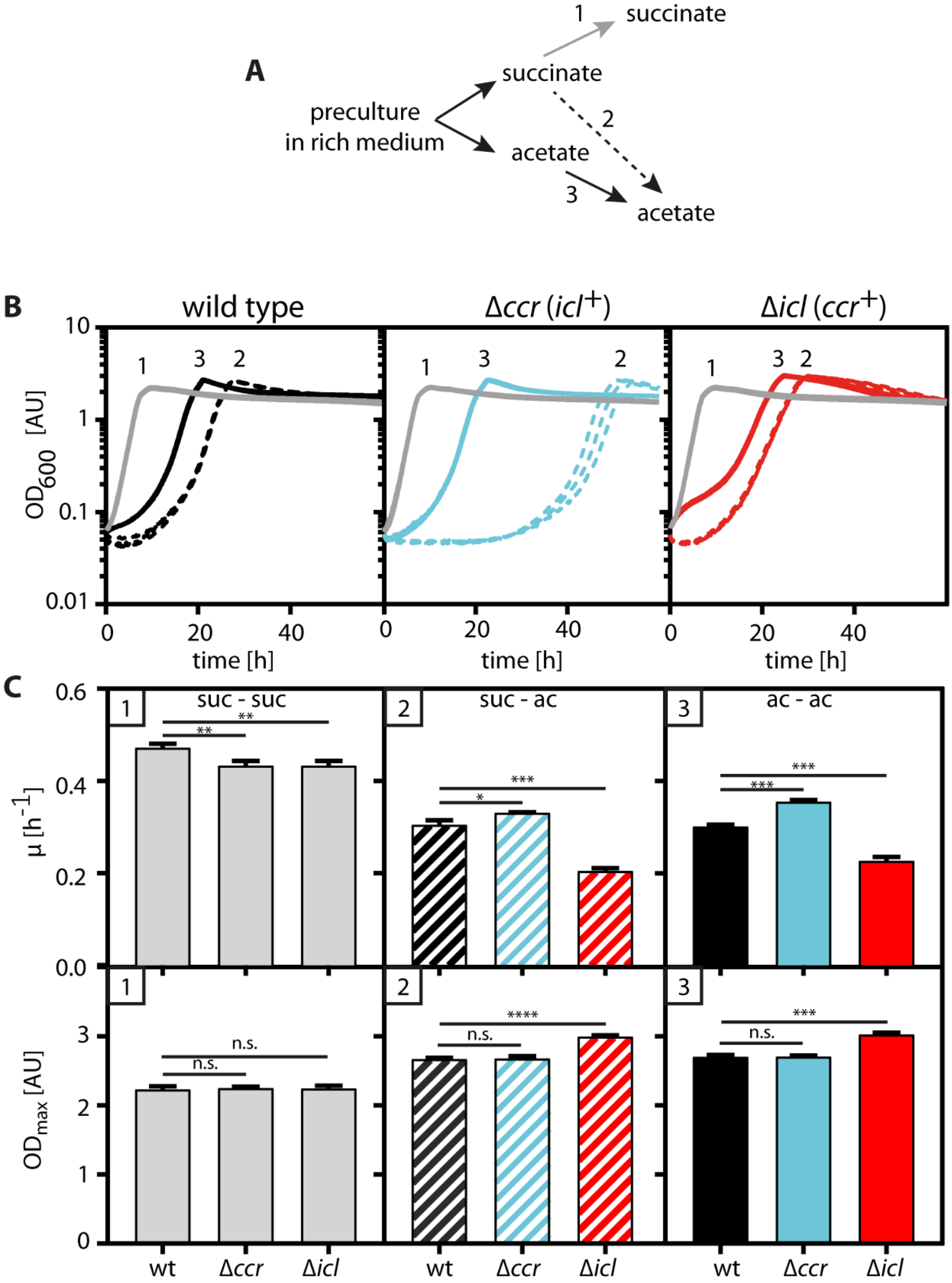
A
preculture
in rich medium
succinate
acetate
1
succinate
2
3
acetate
B
wild type
Δccr (icl+)
Δicl (ccr+)
OD600 [AU]
time [h]
C
suc - suc
suc - ac
ac - ac
μ [h-1]
ODmax [AU]
n.s.
wt
Δccr
Δicl

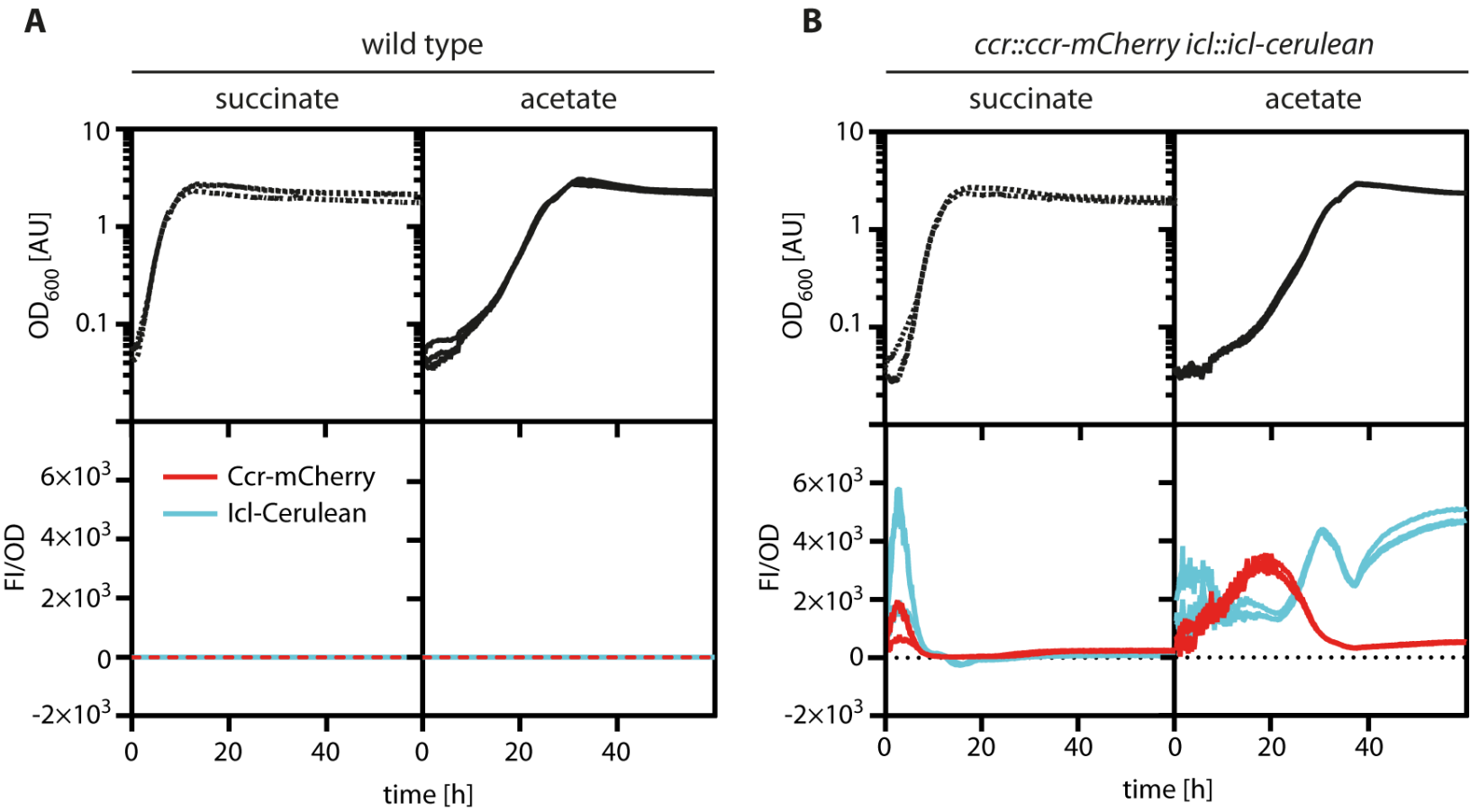
A
wild type
succinate
acetate
10
1
0.1
OD600 [AU]
6×10^3
4×10^3
2×10^3
0
-2×10^3
FI/OD
Ccr-mCherry
Icl-Cerulean
0
20
40
time [h]
B
ccr::ccr-mCherry icl::icl-cerulean
succinate
acetate
time [h]

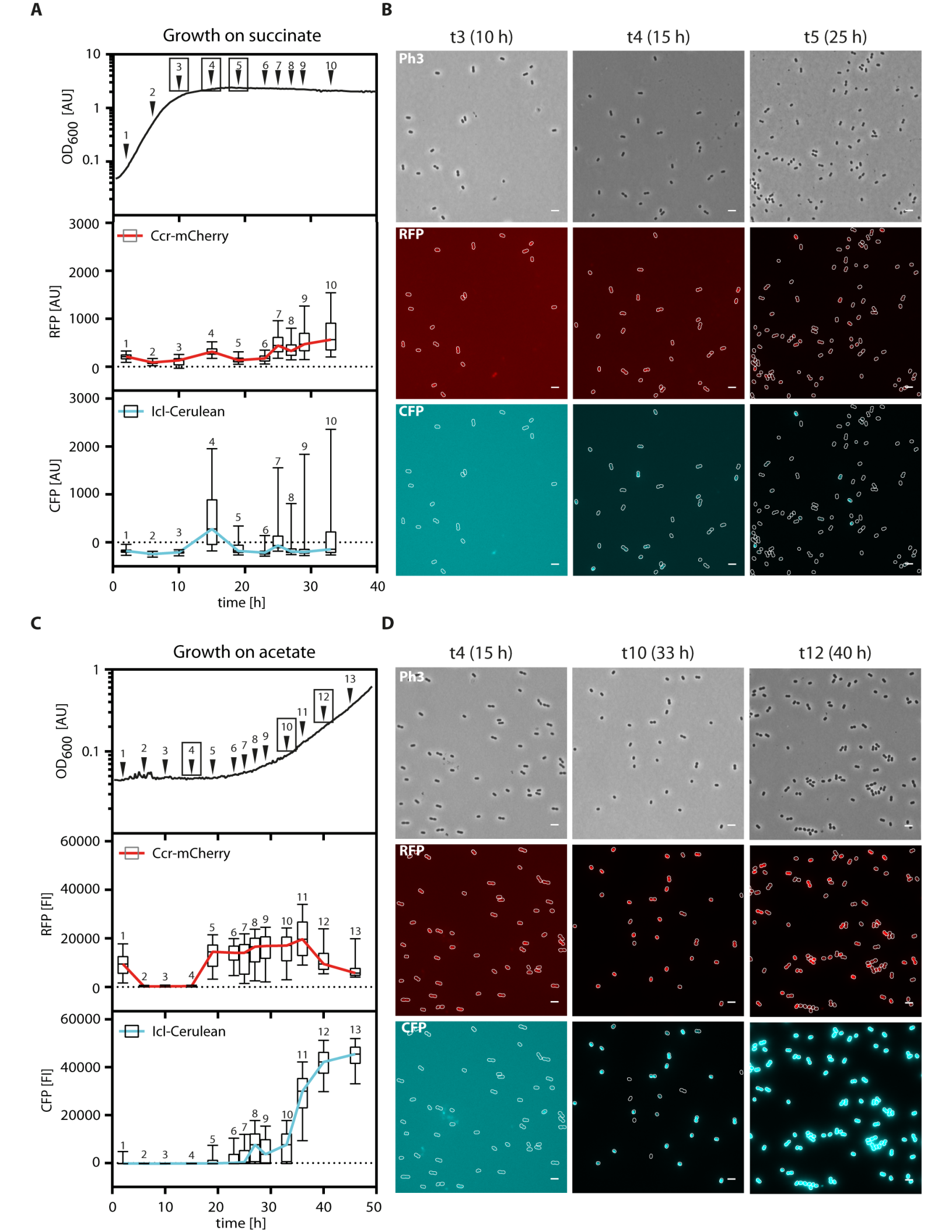
A
Growth on succinate
OD600 [AU]
Ccr-mCherry
RFP [AU]
Icl-Cerulean
CFP [AU]
time [h]
B
t3 (10 h)
t4 (15 h)
t5 (25 h)
Ph3
RFP
CFP
C
Growth on acetate
OD600 [AU]
Ccr-mCherry
RFP [FI]
Icl-Cerulean
CFP [FI]
time [h]
D
t4 (15 h)
t10 (33 h)
t12 (40 h)
Ph3
RFP
CFP

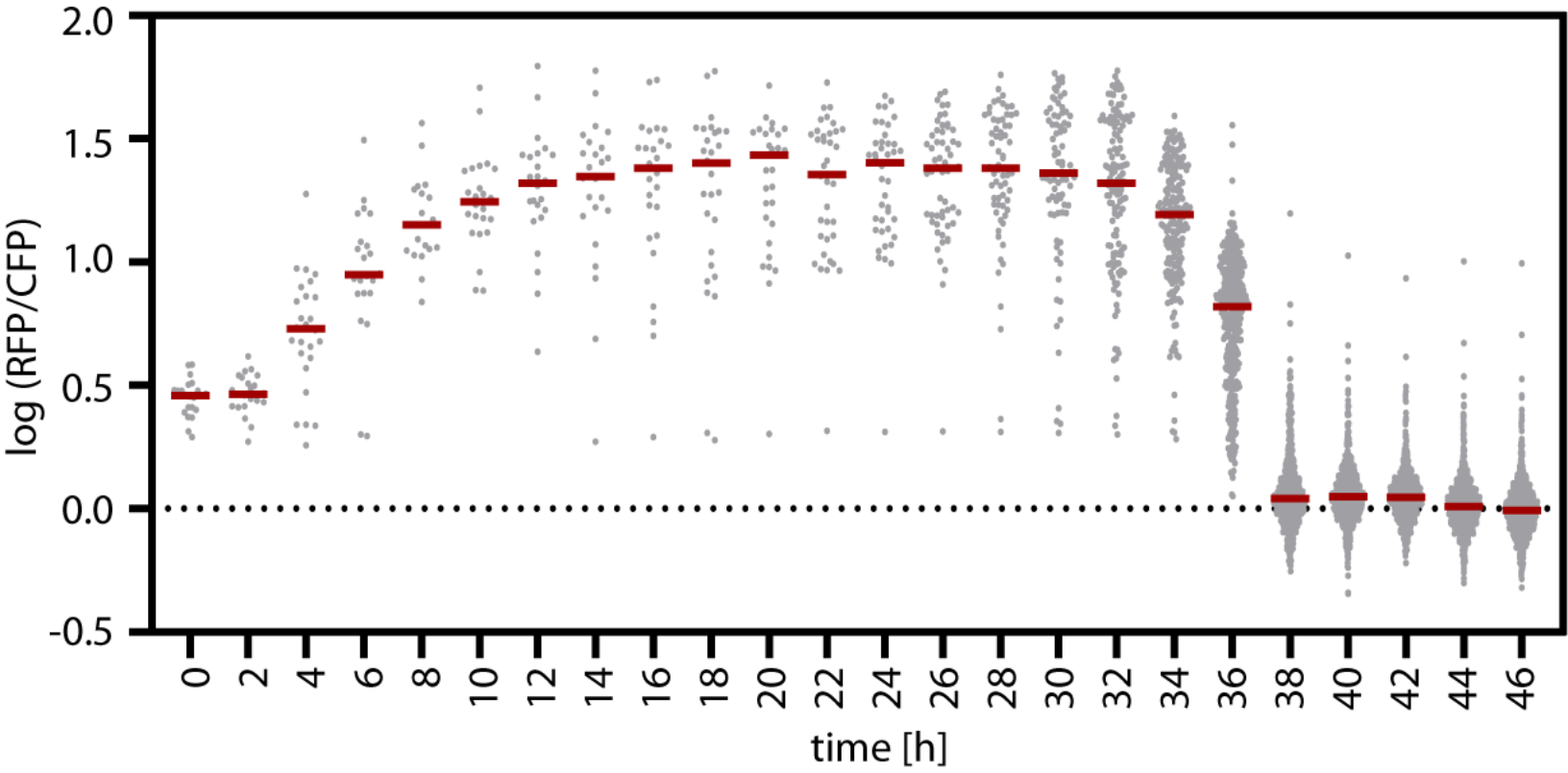
2.0
1.5
1.0
0.5
0.0
-0.5
log (RFP/CFP)
0
2
4
6
8
10
12
14
16
18
20
22
24
26
28
30
32
34
36
38
40
42
44
46
time [h]

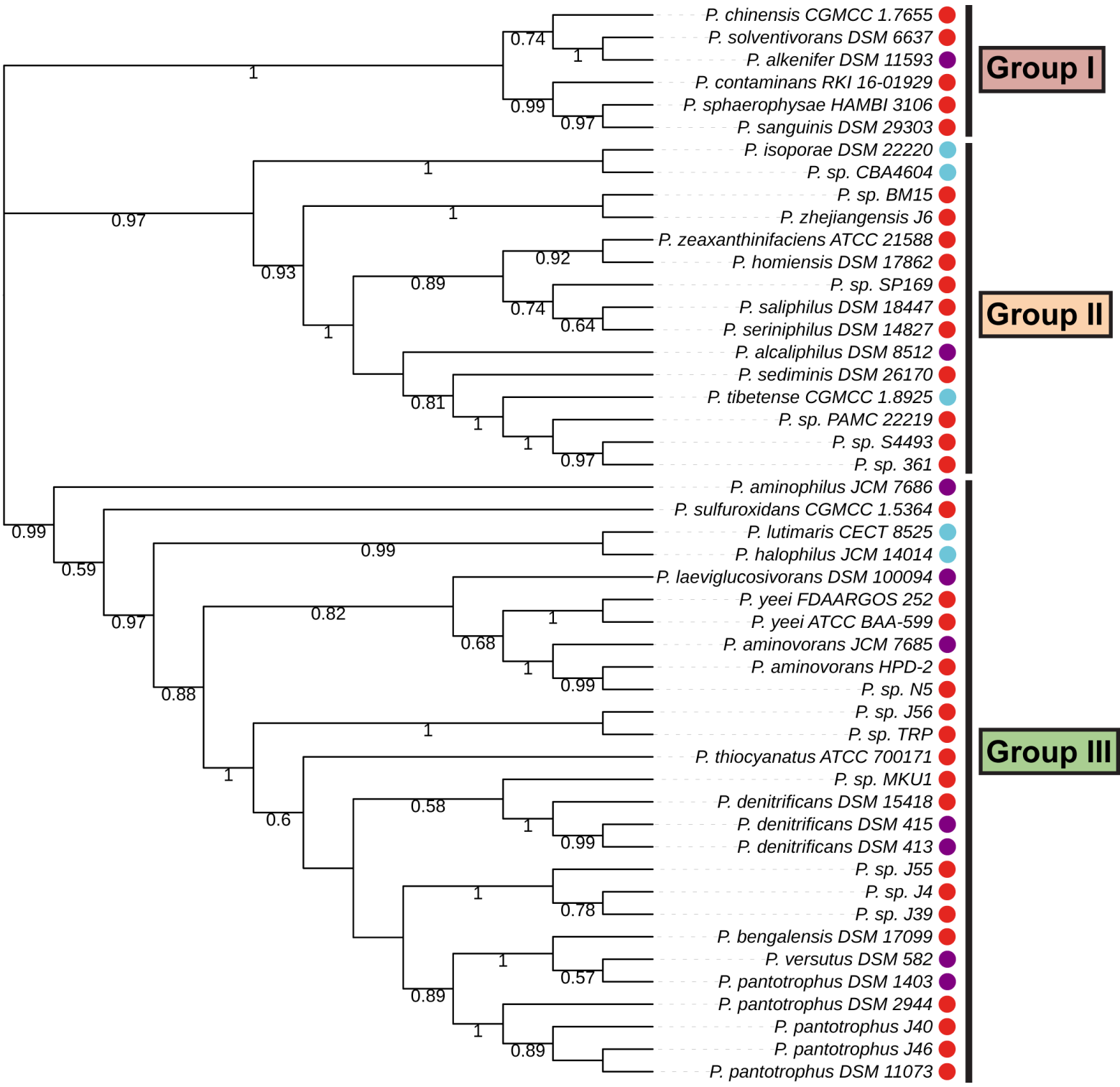
P. chinensis CGMCC 1.7655
P. solventivorans DSM 6637
P. alkenifer DSM 11593
P. contaminans RKI 16-01929
P. sphaerophysae HAMBI 3106
P. sanguinis DSM 29303
P. isoporae DSM 22220
P. sp. CBA4604
P. sp. BM15
P. zhejiangensis J6
P. zeaxanthinifaciens ATCC 21588
P. homiensis DSM 17862
P. sp. SP169
P. saliphilus DSM 18447
P. seriniphilus DSM 14827
P. alcaliphilus DSM 8512
P. sediminis DSM 26170
P. tibetense CGMCC 1.8925
P. sp. PAMC 22219
P. sp. S4493
P. sp. 361
P. aminophilus JCM 7686
P. sulfuroxidans CGMCC 1.5364
P. lutimaris CECT 8525
P. halophilus JCM 14014
P. laeviglucosivorans DSM 100094
P. yeei FDAARGOS 252
P. yeei ATCC BAA-599
P. aminovorans JCM 7685
P. aminovorans HPD-2
P. sp. N5
P. sp. J56
P. sp. TRP
P. thiocyanatus ATCC 700171
P. sp. MKU1
P. denitrificans DSM 15418
P. denitrificans DSM 415
P. denitrificans DSM 413
P. sp. J55
P. sp. J4
P. sp. J39
P. bengalensis DSM 17099
P. versutus DSM 582
P. pantotrophus DSM 1403
P. pantotrophus DSM 2944
P. pantotrophus J40
P. pantotrophus J46
P. pantotrophus DSM 11073
Group I
Group II
Group III